Electron-Transfer Series of $MoFe_3S_4$ Double-Cubane Clusters: Electronic Properties of Components and the Structure of $[(C_2H_5)_4N]_5[Mo_2Fe_6S_8(SC_6H_5)_9]$

G. Christou,[1a,b] P. K. Mascharak,[1a] W. H. Armstrong,[1a] G. C. Papaefthymiou,[1c] R. B. Frankel,*[1c] and R. H. Holm*[1a]

Contribution from the Department of Chemistry, Harvard University, Cambridge, Massachusetts 02138, and the Francis Bitter National Magnet Laboratory, Massachusetts Institute of Technology, Cambridge, Massachusetts 02139.
Received September 15, 1981

Abstract: Electronic properties of certain component members of electron-transfer series 1 and 2 formed by the double-cubane clusters $[Mo_2Fe_6S_8(SR)_9]^z$ (1, z = 2- to 5-) and $[Mo_2Fe_6S_8(\mu_2\text{-}OMe)_3(S\text{-}t\text{-}Bu)_6]^z$ (2, z = 1- to 5-) have been investigated. The series are generated by one-electron reactions of $MoFe_3S_4$ subclusters, which are usually reversible by cyclic voltammetry; 3-, 4-, and 5- members are the more stable and have been produced in solution by electrochemical and chemical reactions. The 5- member of series 1 with R = Ph has been isolated. $(Et_4N)_5[Mo_2Fe_6S_8(SPh)_9]$ crystallizes in monoclinic space group $P2_1/c$ with a = 18.937 (2) Å, b = 26.637 (3) Å, c = 22.534 (2) Å, β = 94.30 (2)°, and Z = 4; the structure was refined to R = 6.6% by using 6517 unique data ($F_0^2 > 2.5\sigma(F_0^2)$). The cluster retains the double-cubane structure of $[Mo_2Fe_6S_8(SR)_9]^{3-}$ species but with an increased Mo···Mo separation and subcluster dimensional changes (e.g., a mean volume increase of 2.6%) consistent with reduction. Isomer shifts derived from fits of low-temperature Mössbauer spectra have been used to follow changes in subcluster charge distribution in series 1. The mean oxidation states $Fe^{2.67+}$ and $Fe^{2.33+}$ are considered the most probable for the 3- and 5- clusters, respectively, of these series. The 4- member of series 1 is concluded to possess (on the Mössbauer time scale at $T \leq 80$ K) inequivalent subclusters containing $Fe^{2.67+}$ and $Fe^{2.33+}$. Absorption spectra and magnetic properties are consistent with this assignment. Collective spectroscopic and redox potential properties serve to demonstrate that electronic structural changes attendant to 3-/4- and 4-/5- electron-transfer reactions of double cubanes are largely confined to subcluster Fe_3 portions and associated sulfur atoms. Assigned (mean) oxidation states of Fe and Mo atoms are intended as the best available estimates of charge distribution rather than precise descriptions.

The Mo-Fe-S clusters $[Mo_2Fe_6S_8(SR)_9]^{3-}$,[2-6] whose bridged double-cubane structure **1**[2,7,8] is well established, have occasioned

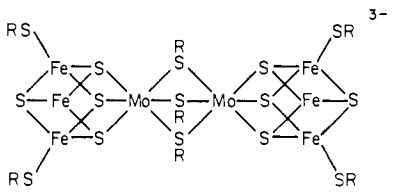

1

considerable current interest as preliminary models of the Mo coordination site(s) in FeMo proteins of nitrogenase and in the FeMo cofactor obtained therefrom.[2] Similar interest attends the bridged double cubanes $[Mo_2Fe_6S_9(SEt)_8]^{3-}$,[2,9] and $[Mo_2Fe_7S_8(SR)_{12}]^{3-,4-}$.[3,10] The Fe(III)-bridged species of the latter type serve as precursors for $[MoFe_4S_4(SR)_3(C_6H_4O_2)_3]^{3-}$ and the new double cubanes $[Mo_2Fe_6S_8(SR)_6(3,6\text{-}R_2'C_6H_2O_2)_2]^{4-}$[12] from which magnetically uncoupled $S = {}^3/_2$ $MoFe_3S_4$-type clusters have been obtained.[12]

Detailed studies of the foregoing clusters have centered on those oxidation levels obtained directly by synthesis, e.g., the trianion form of **1**. However, all of these clusters have the common characteristic of redox properties which generate electron-transfer series whose members are interconverted by one-electron reactions. Thus electrochemical studies of the cluster **1** have demonstrated the existence of the electron-transfer series 3-, 4-, 5-, whose steps appear chemically reversible by cyclic voltammetry. The reduced forms of these and other clusters are most pertinent in the biological model context, and several encouraging results have already been obtained. A water-soluble version of **1** has been found to be capable of replacing ferredoxin in an illuminated chloroplast/hydrogenase H_2-evolving system.[13] More directly related to the nitrogenase model problem is the recent demonstration of one type of reductive substrate reaction by a reduced cluster **1**, viz., H_2 evolution from protic molecules by $[Mo_2Fe_6S_8(SPh)_9]^{5-}$.[14] Complementary to our continuing studies of reactions of reducible substrates with reduced clusters is the present investigation, directed at assessing the electronic and structural properties of such clusters. Described here are certain electrochemical and spectroscopic features of members of the foregoing series and the synthesis and structure of $(Et_4N)_5[Mo_2Fe_6S_8(SPh)_9]$. One purpose of this work is to provide information necessary for an ultimate electronic structural description of component clusters of this series. Included are experimental results related to electronic distribution in clusters of different oxidation levels and to intramolecular electron transfer in species whose $MoFe_3S_4$ subclusters are of formally unequal oxidation levels.

Experimental Section

Preparation of Compounds. The following compounds were obtained by published procedures: $(Et_4N)_3[Mo_2Fe_6S_8(SR)_9]$ (R = Et,[2,5] CH_2CH_2OH,[4] $p\text{-}C_6H_4Me$[5]), $(Et_4N)_3[Mo_2Fe_6S_8(\mu_2\text{-}SEt)_3(SCH_2CH_2OH)_6]$,[4] $(n\text{-}Bu_4N)_3[Mo_2Fe_6S_8(SR)_9]$ (R = Ph, $p\text{-}C_6H_4Cl$[5]), $(Et_4N)_3[Mo_2Fe_6S_8$-

(1) (a) Harvard University. (b) U.K. Science Research Council/NATO Postdoctoral Fellow, 1980-1981. (c) Francis Bitter National Magnet Laboratory.
(2) Wolff, T. E.; Berg, J. M.; Hodgson, K. O.; Frankel, R. B.; Holm, R. H. *J. Am. Chem. Soc.* **1979**, *101*, 4140.
(3) Wolff, T. E.; Power, P. P.; Frankel, R. B.; Holm, R. H. *J. Am. Chem. Soc.* **1980**, *102*, 4694.
(4) Palermo, R. E.; Power, P. P.; Holm, R. H. *Inorg. Chem.* **1982**, *21*, 173.
(5) Christou, G.; Garner, C. D. *J. Chem. Soc., Dalton Trans.* **1980**, 2354.
(6) Christou, G.; Garner, C. D.; Miller, R. M.; Johnson, C. E.; Rush, J. D. *J. Chem. Soc., Dalton Trans.* **1980**, 2363.
(7) Christou, G.; Garner, C. D.; Mabbs, F. E.; King, T. J. *J. Chem. Soc., Chem. Commun.* **1978**, 740.
(8) Acott, S. R.; Christou, G.; Garner, C. D.; King, T. J.; Mabbs, F. E.; Miller, R. M. *Inorg. Chim. Acta* **1979**, *35*, L337.
(9) Wolff, T. E.; Berg, J. M.; Warrick, C.; Hodgson, K. O.; Holm, R. H.; Frankel, R. B. *J. Am. Chem. Soc.* **1978**, *100*, 4630.
(10) Wolff, T. E.; Berg, J. M.; Power, P. P.; Hodgson, K. O.; Holm, R. H. *Inorg. Chem.* **1980**, *19*, 430.
(11) Wolff, T. E.; Berg, J. M.; Holm, R. H. *Inorg. Chem.* **1981**, *20*, 174.
(12) Armstrong, W. H.; Holm, R. H. *J. Am. Chem. Soc.* **1981**, *103*, 6246.
(13) Adams, M. W. W.; Rao, K. K.; Hall, D. O.; Christou, G.; Garner, C. D. *Biochim. Biophys. Acta* **1980**, *589*, 1.
(14) Christou, G.; Hageman, R. V.; Holm, R. H. *J. Am. Chem. Soc.* **1980**, *102*, 7600. Yamamura, T.; Christou, G.; Holm, R. H., work in progress.

0002-7863/82/1504-2820$01.25/0

$(\mu_2\text{-OMe})_3(SPh)_6]$,[5] $(Et_4N)_3[Mo_2Fe_6S_9(SEt)_8]$,[2] $(Ph_3PCH_2Ph)_2[Fe_4S_4(SCH_2Ph)_4]$,[15] $(Me_4N)_2[Fe_4S_4(SR)_4]$ (R = *p*-C_6H_4Me,[16] SCH_2CH_2OH[17,18]), (*n*-$Bu_4N)_2[Fe_4S_4(SR)_4]$ (R = Et, *t*-Bu, Ph;[15,18] *p*-C_6H_4Cl[19]), and $(Ph_4As)_2[Fe_4S_4(S\text{-}p\text{-}C_6H_4OMe)_4]$.[20]

In the following preparations, degassed solvents were used and all manipulations were performed under a pure argon or dinitrogen atmosphere.

(*n*-$Bu_4N)_3[Mo_2Fe_6S_8(S\text{-}p\text{-}C_6H_4OMe)_9]$. A previous procedure[5] was used, which afforded the compound as thin black needles in 59% yield after recrystallization from acetonitrile/methanol. Anal. Calcd for $C_{111}H_{171}Fe_6Mo_2N_3O_9S_{17}$: C, 48.24; H, 6.24; N, 1.52; S, 19.72. Found: C, 48.22; H, 6.36; N, 1.49; S, 19.42.

(*n*-$Pr_4N)_3[Mo_2Fe_6S_8(SCH_2Ph)_9]$. A previous procedure[5] was employed except that the $NaSCH_2Ph$ solution was added to the $FeCl_3$ solution (not the reverse), in order to prevent formation of the insoluble and relatively unreactive iron thiolate. The crude product was collected and was recrystallized from acetonitrile/methanol, affording the pure product (5.4 g, 44%) as black crystals. Anal. Calcd for $C_{99}H_{147}Fe_6Mo_2N_3S_{17}$: C, 48.51; H, 6.05; N, 1.71; S, 22.23. Found: C, 48.70; H, 6.10; N, 1.61; S, 21.93.

$(Et_4N)_3[Mo_2Fe_6S_8(\mu_2\text{-OMe})_3(S\text{-}t\text{-Bu})_6]$. A solution of 4.87 g (30 mmol) of $FeCl_3$ in 60 mL of methanol was added to a solution of 90 mmol of NaS-*t*-Bu (from 2.07 g of sodium and 8.12 g of *tert*-butyl mercaptan) in 70 mL of methanol, giving a reddish-brown solution and some off-white solid. Addition of 2.60 g (10 mmol) of solid $(NH_4)_2MoS_4$[21] caused a color change to deep greenish brown. After the solution was stirred overnight, the reaction mixture was filtered into a stirred solution of 6.30 g (30 mmol) of Et_4NBr in 20 mL of methanol. The resultant black microcrystalline precipitate was collected, washed with methanol, and dried in vacuo. This material was dissolved in 300 mL of warm (~60 °C) acetonitrile, and the solution was filtered. THF (140 mL) was added to the filtrate. This solution was cooled slowly to ambient temperature and then was maintained overnight at −20 °C. Pure product (3.82 g, 42%) was isolated in the form of long black needles; ^1H NMR ($Me_2SO\text{-}d_6$, 23 °C) −7.31 (*t*-Bu), +3.07 ppm (OMe). Anal. Calcd for $C_{51}H_{123}Fe_6Mo_2N_3O_3S_{14}$: C, 33.99; H, 6.88; Fe, 18.59; Mo, 10.65; N, 2.33; S, 24.90. Found: C, 34.06; H, 6.91; Fe, 18.44; Mo, 10.71; N, 2.23; S, 24.64.

$(Et_4N)_5[Mo_2Fe_6S_8(SPh)_9]$. A solution of 4.99 g (2.06 mmol) of (*n*-$Bu_4N)_3[Mo_2Fe_6S_8(SPh)_9]$ and 4.20 g (20 mmol) of dry Et_4NBr in 100 mL of acetonitrile was treated with 3 equiv of a 0.5 M solution of sodium acenaphthylenide in HMPA (or THF) under an Ar atmosphere. The solution color rapidly changed from red-brown to green-brown, and a crystalline solid separated. After the reaction mixture was stored at −20 °C overnight, the solid was collected and recrystallized from 100 mL of acetonitrile heated initially to 60 °C. The pure product (2.1–2.3 g, 44–48%) was isolated as well-formed black prisms which are extremely sensitive to dioxygen. Anal. Calcd for $C_{94}H_{145}Fe_6Mo_2N_5S_{17}$: C, 46.71; H, 6.05; Fe, 13.86; Mo, 7.94; N, 2.90; S, 22.55. Found: C, 46.62; H, 5.98; Fe, 13.90; Mo, 8.00; N, 3.03; S, 22.33.

Physical Measurements. Owing to the air sensitivity of all compounds, measurements were performed under strictly anaerobic conditions. Solvents were purified as follows: DMF, dried over 3-Å molecular sieves and freshly distilled from CaH_2; *N,N'*-dimethylacetamide (DMA), dried over CaH_2 and distilled 3 times from sodium acenaphthylenide solution; acetonitrile-d_3, distilled in succession from alkaline $KMnO_4$, $KHSO_4$, and CaH_2 and then trap-to-trap distilled from $(Et_4N)_5[Mo_2Fe_6S_8(SPh)_9]$. Absorption spectra were recorded on a Cary Model 219 or 17 spectrophotometer. Spectroelectrochemical experiments were performed by using an OTTLE cell described elsewhere.[22] Electrochemical measurements were made with standard Princeton Applied Research instrumentation using a Pt or glassy carbon working electrode. Solutions contained 0.1 M (*n*-$Bu_4N)(ClO_4)$ supporting electrolyte. Potentials were determined at 25 °C vs. a saturated calomel electrode (SCE). ^1H NMR spectra were recorded on a Brüker WM-300 spectrometer equipped with a deuterium lock. Chemical shifts downfield and upfield of Me_4Si are designated as negative and positive, respectively, for paramagnetic clusters. Solution magnetic susceptibilities were determined by the conventional NMR method using Me_4Si solution and reference shift differences measured to ±0.2 Hz, ca. 1 mM cluster solutions in CD_3CN, and coaxial tubes. Solid samples were measured with a SQUID susceptometer using the procedures described.[23] All susceptibility data were corrected for diamagnetism. Mössbauer spectra were measured by using equipment and procedures specified earlier.[3,23] Polycrystalline samples were dispersed in boron nitride powder. For solution measurements (*n*-$Bu_4N)_3[Mo_2{}^{57}Fe_6S_8(SPh)_9]$ (95 atom % ^{57}Fe) was prepared by the method for the unenriched compound.[5] Solutions of $[Mo_2{}^{57}Fe_6S_8(SPh)_9]^{5-}$ (~1 mM) were prepared by reaction of 1.0 equiv of the cluster trianion in DMA with 2.2 equiv of sodium acenaphthylenide ($E_{1/2} \simeq$ −1.7 V[24]) in HMPA. Solutions of $[Mo_2{}^{57}Fe_6S_8(SPh)_9]^{4-}$ (~1 mM, ~48% enriched) were produced by the reaction of exactly equimolar quantities of $[Mo_2{}^{57}Fe_6S_8(SPh)_9]^{3-}$ and $[Mo_2Fe_6S_8(SPh)_9]^{5-}$ in DMA solution. Absorption spectra of 5- and 4- cluster solutions were virtually identical with those obtained by generation of these species in the OTTLE cell. Solutions of $[Mo_2Fe_6S_9(SEt)_8]^{5-}$ (~5 mM) were obtained by reduction of $(Et_4N)_3[Mo_2Fe_6S_9(SEt)_8]$ in DMA with 3.0 equiv of sodium acenaphthylenide. Spectra of these 3- and 5- clusters were obtained on unenriched samples. Solutions for Mössbauer spectral measurements were frozen immediately after preparation. All ^{57}Fe isomer shifts are quoted vs. Fe metal reference at the same temperature as the absorber.

Table I. Summary of Crystal Data, Intensity Collection, and Structure Refinement Parameters for $(Et_4N)_5[Mo_2Fe_6S_8(SPh)_9]$

formula (mol wt)	$C_{94}H_{145}Fe_6Mo_2N_5S_{17}$ (2417.29)
a, Å	18.937 (2)
b, Å	26.637 (3)
c, Å	22.534 (2)
β, deg	94.30 (2)
cryst. system	monoclinic
V, Å^3	11 334 (3)
Z	4
d_{calcd}, g/cm^3	1.42
d_{obsd}, g/cm^3	1.42[a]
space group	$P2_1/c$
cryst. dimensions,[b] mm	0.49 × 0.40 × 0.09
cryst. faces	(100), ($\bar{1}$00), (01$\bar{1}$), (0$\bar{1}$1), (011), (0$\bar{1}\bar{1}$)
radiation	Mo K$\bar{\alpha}$ (λ 0.71069 Å)
absorption coeff., μ, cm^{-1}	13.0
scan speed, deg/min	2.0–29.3 ($\theta/2\theta$ scan)
scan range, deg	1.6 + ($2\theta_{K\alpha_2}$−$2\theta_{K\alpha_1}$)
background/scan time ratio	0.25
data collected	2θ of 4–42°; $+h,+k,\pm l$
unique data ($F_o^2 > 2.5\sigma(F_o^2)$)	6517
no. of variables	820
goodness of fit	1.25
R, %	6.60
R_w, %	6.99

[a] Determined by flotation in CCl_4/EtOAc. [b] Platelike crystal.

Collection and Reduction of X-ray Data. A black air-sensitive crystal of $(Et_4N)_5[Mo_2Fe_6S_8(SPh)_9]$ was mounted in a glass capillary under an argon atmosphere. Diffraction experiments were performed on a Nicolet R3M four-circle automated diffractometer with a Mo X-ray tube equipped with a graphite monochromator. The machine parameters are summarized in Table I. The orientation matrix was determined by using 25 machine-centered reflections which had 2θ values between 15° and 20°. The crystal showed ω scans with full width at half-height of ~0.3°. Throughout the data collection three standard reflections were recorded after every 60 reflections. No significant decay in these reflections was observed. The parameters used in data collection are listed in Table I. Data reduction was performed with the program XTAPE of the SHELXTL program package. A numerical absorption correction was applied. The compound belongs to the monoclinic system; the systematic absences $0k0$ ($k \neq 2n$) and $h0l$ ($l \neq 2n$) are consistent only with space group $P2_1/c$. Subsequent solution and refinement of the structure confirmed this assignment.

Solution and Refinement of the Structure. The structure was solved by use of the direct methods program MULTAN. The *E* map from the phase set with the highest combined figure of merit yielded trial positions

(15) Averill, B. A.; Herskovitz, T.; Holm, R. H.; Ibers, J. A. *J. Am. Chem. Soc.* **1973**, *95*, 3523.
(16) Holm, R. H.; Phillips, W. D.; Averill, B. A.; Mayerle, J. J.; Herskovitz, T. *J. Am. Chem. Soc.* **1974**, *96*, 2109.
(17) Hill, C. L.; Renaud, J.; Holm, R. H.; Mortenson, L. E. *J. Am. Chem. Soc.* **1977**, *99*, 2549.
(18) Christou, G.; Garner, C. D. *J. Chem. Soc., Dalton Trans.* **1979**, 1093.
(19) Mayerle, J. J.; Denmark, S. E.; DePamphilis, B. V.; Ibers, J. A.; Holm, R. H. *J. Am. Chem. Soc.* **1975**, *97*, 1032.
(20) Hill, C. L.; Steenkamp, D. J.; Holm, R. H.; Singer, T. P. *Proc. Natl. Acad. Sci. U.S.A.* **1977**, *94*, 547.
(21) Krüss, G. *Justus Liebigs Ann. Chem.* **1884**, *225*, 6.
(22) Stolzenberg, A. M.; Spreer, L. O.; Holm, R. H. *J. Am. Chem. Soc.* **1980**, *102*, 364.
(23) Laskowski, E. J.; Frankel, R. B.; Gillum, W. O.; Papaefthymiou, G. C.; Renaud, J.; Ibers, J. A.; Holm, R. H. *J. Am. Chem. Soc.* **1978**, *100*, 5322.
(24) Mascharak, P. K.; Papaefthymiou, G. C.; Frankel, R. B.; Holm, R. H. *J. Am. Chem. Soc.* **1981**, *103*, 6110.

Table II. Positional and Thermal Parameters[a] for $[Mo_2Fe_6S_8(SPh)_9]^{5-}$

atom	x	y	z	U_{11}[c]	U_{22}	U_{33}	U_{23}	U_{13}	U_{12}
Mo(1)	0.01420 (6)[b]	0.16136 (5)	0.27434 (5)	28 (1)	40 (1)	32 (1)	−1 (1)	3 (1)	−2 (1)
Mo(2)	−0.18393 (6)	0.17221 (5)	0.23169 (5)	29 (1)	33 (1)	32 (1)	3 (1)	6 (1)	1 (1)
Fe(1)	0.1200 (1)	0.1381 (1)	0.3601 (1)	34 (1)	64 (2)	32 (1)	−3 (1)	−2 (1)	3 (1)
Fe(2)	0.1456 (1)	0.2076 (1)	0.2777 (1)	36 (2)	61 (2)	44 (2)	−8 (1)	8 (1)	−12 (1)
Fe(3)	0.1341 (1)	0.1082 (1)	0.2479 (1)	38 (2)	53 (2)	40 (1)	−4 (1)	8 (1)	4 (1)
Fe(4)	−0.2952 (1)	0.1373 (1)	0.1563 (1)	39 (2)	56 (2)	41 (1)	−1 (1)	3 (1)	−9 (1)
Fe(5)	−0.2893 (1)	0.2357 (1)	0.1874 (1)	37 (2)	48 (2)	45 (1)	10 (1)	3 (1)	5 (1)
Fe(6)	−0.3197 (1)	0.1646 (1)	0.2667 (1)	32 (1)	49 (2)	43 (1)	4 (1)	10 (1)	0 (1)
S(1)	0.0678 (2)	0.2145 (2)	0.3498 (2)	38 (3)	55 (3)	44 (3)	−15 (2)	0 (2)	−1 (2)
S(2)	0.0885 (2)	0.1752 (2)	0.1951 (2)	42 (3)	54 (3)	38 (3)	1 (2)	8 (2)	−6 (2)
S(3)	0.0509 (2)	0.0812 (2)	0.3076 (2)	36 (3)	45 (3)	42 (3)	3 (2)	6 (2)	3 (2)
S(4)	0.2217 (2)	0.1438 (2)	0.3095 (2)	30 (3)	82 (4)	54 (3)	−8 (3)	5 (2)	3 (2)
S(5)	0.1347 (2)	0.1064 (2)	0.4560 (2)	52 (3)	91 (4)	36 (3)	3 (3)	−2 (2)	10 (3)
S(6)	0.2020 (3)	0.2798 (2)	0.2510 (2)	74 (4)	71 (4)	68 (3)	−3 (3)	8 (3)	−29 (3)
S(7)	0.1638 (3)	0.0341 (2)	0.2049 (2)	106 (5)	60 (3)	69 (4)	−2 (3)	34 (3)	17 (3)
S(8)	−0.0735 (2)	0.2308 (2)	0.2284 (2)	35 (2)	42 (3)	34 (2)	6 (2)	2 (2)	−4 (2)
S(9)	−0.0810 (2)	0.1146 (2)	0.2052 (2)	37 (2)	47 (3)	37 (2)	−6 (2)	6 (2)	0 (2)
S(10)	−0.1016 (2)	0.1593 (2)	0.3307 (2)	34 (2)	46 (3)	30 (2)	7 (2)	4 (2)	2 (2)
S(11)	−0.2520 (2)	0.0987 (2)	0.2415 (2)	39 (3)	41 (3)	47 (3)	1 (2)	8 (2)	−3 (2)
S(12)	−0.2476 (2)	0.2323 (2)	0.2841 (2)	42 (3)	42 (3)	37 (2)	−2 (2)	10 (2)	3 (2)
S(13)	−0.2137 (2)	0.1947 (2)	0.1311 (2)	40 (3)	49 (3)	31 (2)	9 (2)	3 (2)	−2 (2)
S(14)	−0.3889 (2)	0.1858 (2)	0.1809 (2)	30 (3)	72 (3)	65 (3)	4 (3)	−2 (2)	−1 (2)
S(15)	−0.3288 (3)	0.0814 (2)	0.0819 (2)	63 (3)	88 (4)	49 (3)	−8 (3)	4 (3)	−23 (3)
S(16)	−0.3145 (3)	0.3125 (2)	0.1440 (2)	64 (3)	59 (3)	65 (3)	22 (3)	7 (3)	12 (3)
S(17)	−0.3846 (3)	0.1355 (2)	0.3411 (2)	76 (4)	120 (5)	81 (4)	17 (3)	34 (3)	−19 (4)

[a] Carbon atoms not included. [b] Estimated standard deviations in parentheses in this and succeeding tables. [c] The form of the thermal ellipsoid is $\exp[-2\pi^2(U_{11}h^2a^{*2} + U_{22}k^2b^{*2} + U_{33}l^2c^{*2} + 2U_{12}hka^*b^* + 2U_{13}hla^*c^* + 2U_{23}klb^*c^*]$; quantities given are thermal coefficients $\times 10^3$.

for the Mo and Fe atoms. The remaining nonhydrogen atoms were located from subsequent difference Fourier maps. The structure was refined by blocked-cascade least-squares refinement. Calculated fixed contributions from hydrogen atoms of the eight ordered phenyl rings of the anion were included in the final refinement cycles, with thermal parameters set at 1.2 times that of the bonded carbon atom. The asymmetric unit consists of the anion and five cations. The Mo, Fe, and S atoms were refined anisotropically, and the C atoms of the anion were refined isotropically. The phenyl ring of one ligand (S(17)Ph) was found to be disordered in two positions having a 3:2 occupancy ratio, with apparent S–C distances (1.57, 1.62 Å) that were short compared to normal values (~1.76 Å[25]). The majority rings were well-behaved during refinement whereas the minority ring shifted considerably. Of the five cations, three (1, 2, 3) were well-ordered and were refined anisotropically. The other two cations (4, 5) evidenced disorder and were refined isotropically. Cation 4 was disordered such that several regions of electron density were present near the expected position of one of the four methyl carbon atoms. Refinement using three methyl carbon positions in a 1:1:1 ratio gave long C–C distances (1.81–2.18 Å). Cation 5 exhibited one well-ordered ethyl group. The remaining groups were modeled by a total of five methylene and six methyl carbon atom positions. For the partially occupied positions ranges of C–N and C–C distances were 1.51–1.68 and 1.46–1.78 Å, respectively. Subsequent difference Fourier maps showed no peaks close to cations 4 and 5 that were greater than ~40% of the height of a carbon atom. In the refinements, data for which $F_o^2 > 2.5\sigma(F_o)^2$ were used, giving the ratio NO:NV = 7.95 where NO is the number of observations and NV the number of variables refined. The goodness of fit (GOF) = $[\sum w(|F_o| - |F_c|)^2/(NO - NV)]^{1/2}$; $w = [(\sigma(F_o))^2 + 0.0025(F_o)^2]^{-1}$. Final R factors are given in Table I.

The following results for $(Et_4N)_5[Mo_2Fe_6S_8(SPh)_9]$ are tabulated: positional and thermal parameters for the anion (Table II), selected interatomic distances and angles in the anion (Table III), unit-weighted least-squares planes for the anion (Table S-I), positional and thermal parameters for benzenethiolate carbon atoms (Table S-II) and cation carbon and nitrogen atoms (Table S-III), and values of $10|F_o|$ and $10|F_c|$ (Table S-IV). Tables S-I to S-IV are available as supplementary material (see paragraph at the end of this paper).

Results and Discussion

Electron-Transfer Series: Preparation and Generation of Component Clusters. In order to assess the scope of electron-transfer series, develop means of preparing or generating series components for spectroscopic measurements, and examine trends in redox potentials, we have investigated several types of clusters by cyclic voltammetry (CV) and differential pulse polarography (DPP). Because previously reported data from different laboratories for some of the clusters examined here were not obtained under the same conditions,[3,4,6] identical experimental conditions in DMF solutions were employed in this work. Certain results are displayed in Figure 1, and DPP peak potentials (E_p) for all clusters are collected in Table IV.

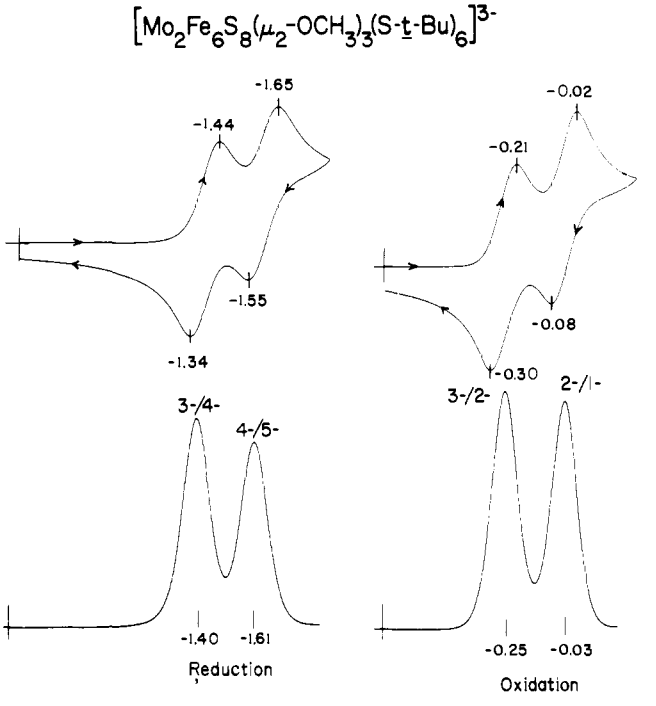

Figure 1. Cyclic voltammograms (100 mV/s) and differential pulse polarograms demonstrating redox reactions of $[Mo_2Fe_6S_8(\mu_2\text{-}OMe)_3(S\text{-}t\text{-}Bu)_6]^{3-}$ in DMF solution leading to 1–, 2–, 4–, and 5– oxidation levels. Peak potentials vs. SCE are indicated.

(a) $[Mo_2Fe_6S_8(SR)_9]^z$ (1). Existence of a four-membered series is apparent from the results for the representative R = Ph system.

(25) Que, L., Jr.; Bobrik, M. A.; Ibers, J. A.; Holm, R. H. *J. Am. Chem. Soc.* **1974**, *96*, 4168.

Table III. Selected Interatomic Distances (Å) and Angles (Deg) in $[Mo_2Fe_6S_8(SPh)_9]^{5-}$

			$Mo(\mu_2\text{-}SPh)_3Mo$ Bridge				
Mo(1)···Mo(2)	3.813 (2)	Mo(1)-S(8)-Mo(2)	93.0	S(8)···S(9)	3.139 (5)	S(8)-Mo(1)-S(9)	73.4 (2)
		Mo(1)-S(9)-Mo(2)	94.5	S(8)···S(10)	3.066 (5)	S(8)-Mo(1)-S(10)	71.3 (2)
Mo(1)-S(8)	2.644 (4)	Mo(1)-S(10)-Mo(2)	92.9	S(9)···S(10)	3.119 (5)	S(9)-Mo(1)-S(10)	73.3 (2)
Mo(1)-S(9)	2.608 (4)	mean	93.5	mean	3.108 (38)	S(8)-Mo(2)-S(9)	74.3 (2)
Mo(1)-S(10)	2.615 (4)					S(8)-Mo(2)-S(10)	71.3 (2)
Mo(2)-S(8)	2.614 (4)					S(9)-Mo(2)-S(10)	73.2 (2)
Mo(2)-S(9)	2.585 (4)					mean	72.8
Mo(2)-S(10)	2.647 (4)						
mean	2.619 (23)[a]						
			$MoFe_3S_4(SPh)_3$ Clusters[b]				
Mo(1)-S(1)	2.381 (4)	S(1)-Mo(1)-S(2)	101.5 (1)	Mo(1)···Fe(1)	2.747 (2)	S(1)-Fe(1)-S(3)	108.5 (2)
Mo(1)-S(2)	2.383 (4)	S(1)-Mo(1)-S(3)	102.3 (1)	Mo(1)···Fe(2)	2.772 (2)	S(1)-Fe(1)-S(4)	105.2 (2)
Mo(1)-S(3)	2.352 (4)	S(2)-Mo(1)-S(3)	101.6 (1)	Mo(1)···Fe(3)	2.778 (2)	S(3)-Fe(1)-S(4)	104.8 (2)
Mo(2)-S(11)	2.365 (4)	S(11)-Mo(2)-S(12)	102.2 (1)	Mo(2)···Fe(4)	2.766 (2)	S(1)-Fe(2)-S(2)	108.9 (2)
Mo(2)-S(12)	2.373 (4)	S(11)-Mo(2)-S(13)	101.9 (1)	Mo(2)···Fe(5)	2.746 (2)	S(1)-Fe(2)-S(4)	105.1 (2)
Mo(2)-S(13)	2.372 (4)	S(12)-Mo(2)-S(13)	102.5 (1)	Mo(2)···Fe(6)	2.753 (2)	S(2)-Fe(2)-S(4)	103.0 (2)
mean	2.371 (11)	mean	102.0	mean	2.760 (14)	S(2)-Fe(3)-S(3)	107.8 (2)
		Mo(1)-S(1)-Fe(1)	72.4 (1)			S(2)-Fe(3)-S(4)	102.8 (2)
Mo(1)-S(4)	3.976 (4)	Mo(1)-S(1)-Fe(2)	72.9 (1)	Fe(1)···Fe(2)	2.690 (3)	S(3)-Fe(3)-S(4)	106.0 (2)
Mo(2)-S(14)	3.980 (4)	Mo(1)-S(2)-Fe(2)	73.4 (1)	Fe(1)···Fe(3)	2.684 (3)	S(11)-Fe(4)-S(13)	107.9 (2)
mean	3.978	Mo(1)-S(2)-Fe(3)	73.2 (1)	Fe(2)···Fe(3)	2.735 (3)	S(11)-Fe(4)-S(14)	106.6 (2)
		Mo(1)-S(3)-Fe(1)	72.8 (1)	Fe(4)···Fe(5)	2.713 (3)	S(13)-Fe(4)-S(14)	103.6 (2)
Fe(1)-S(1)	2.267 (5)	Mo(1)-S(3)-Fe(3)	74.0 (1)	Fe(4)···Fe(6)	2.665 (3)	S(12)-Fe(5)-S(13)	109.3 (2)
Fe(1)-S(3)	2.276 (4)	Mo(2)-S(11)-Fe(4)	73.1 (1)	Fe(5)···Fe(6)	2.696 (3)	S(12)-Fe(5)-S(14)	105.3 (2)
Fe(1)-S(4)	2.315 (5)	Mo(2)-S(11)-Fe(6)	72.8 (1)	mean	2.697 (24)	S(13)-Fe(5)-S(14)	103.6 (2)
Fe(2)-S(1)	2.281 (5)	Mo(2)-S(12)-Fe(5)	72.6 (1)	S(1)···S(2)	3.689 (5)	S(11)-Fe(6)-S(12)	108.3 (2)
Fe(2)-S(2)	2.253 (4)	Mo(2)-S(12)-Fe(6)	72.5 (1)	S(1)···S(3)	3.685 (6)	S(11)-Fe(6)-S(14)	105.9 (2)
Fe(2)-S(4)	2.305 (5)	Mo(2)-S(13)-Fe(4)	73.0 (1)	S(1)···S(4)	3.640 (6)	S(12)-Fe(6)-S(14)	104.1 (2)
Fe(3)-S(2)	2.277 (4)	Mo(2)-S(13)-Fe(5)	72.6 (1)	S(2)···S(3)	3.671 (5)	mean	105.9
Fe(3)-S(3)	2.265 (4)	mean	72.9	S(2)···S(4)	3.567 (5)		
Fe(3)-S(4)	2.288 (4)			S(3)···S(4)	3.636 (5)	Fe(1)-S(4)-Fe(2)	71.2 (1)
Fe(4)-S(11)	2.277 (4)	Fe(1)-S(1)-Fe(2)	72.5 (1)	S(11)···S(12)	3.688 (5)	Fe(1)-S(4)-Fe(3)	71.3 (1)
Fe(4)-S(13)	2.274 (4)	Fe(2)-S(2)-Fe(3)	74.3 (1)	S(11)···S(13)	3.679 (5)	Fe(2)-S(4)-Fe(3)	73.1 (1)
Fe(4)-S(14)	2.295 (5)	Fe(1)-S(3)-Fe(3)	72.5 (1)	S(11)···S(14)	3.666 (6)	Fe(4)-S(14)-Fe(5)	72.3 (1)
Fe(5)-S(12)	2.264 (4)	Fe(4)-S(11)-Fe(6)	71.8 (1)	S(12)···S(13)	3.695 (5)	Fe(4)-S(14)-Fe(6)	70.5 (1)
Fe(5)-S(13)	2.265 (4)	Fe(5)-S(12)-Fe(6)	72.8 (1)	S(12)···S(14)	3.630 (5)	Fe(5)-S(14)-Fe(6)	71.3 (1)
Fe(5)-S(14)	2.304 (5)	Fe(4)-S(13)-Fe(5)	73.4 (1)	S(13)···S(14)	3.590 (6)	mean	71.6
Fe(6)-S(11)	2.271 (4)	mean	72.8	mean	3.653 (41)		
Fe(6)-S(12)	2.280 (4)					Fe(1)-Mo(1)-Fe(2)	58.3 (1)
Fe(6)-S(14)	2.322 (4)			Fe(1)···S(2)	3.849 (4)	Fe(1)-Mo(1)-Fe(3)	58.1 (1)
mean	2.282 (19)			Fe(2)···S(3)	3.897 (4)	Fe(2)-Mo(1)-Fe(3)	59.0 (1)
				Fe(3)···S(1)	3.912 (5)	Fe(4)-Mo(2)-Fe(5)	59.0 (1)
Fe(1)-S(5)	2.318 (4)			Fe(4)···S(12)	3.889 (4)	Fe(4)-Mo(2)-Fe(6)	57.7 (1)
Fe(2)-S(6)	2.303 (5)			Fe(5)···S(11)	3.897 (5)	Fe(5)-Mo(2)-Fe(6)	58.7 (1)
Fe(3)-S(7)	2.288 (5)			Fe(6)···S(13)	3.864 (4)	mean	58.5
Fe(4)-S(15)	2.296 (5)			mean	3.885 (24)		
Fe(5)-S(16)	2.303 (5)						
Fe(6)-S(17)	2.288 (6)						
mean	2.299 (11)						

[a] The standard deviation of the mean was estimated from $\sigma \approx s = [(\Sigma x_i^2 - n\bar{x}^2/(n-1)]^{1/2}$; no value is given for angular quantities, as the variations exceed those expected from a sample taken from the same population. [b] Ranges and mean values of nontabulated quantities. S(cluster)-Mo-S(bridge), 86.1-96.0°, 90.9° (12 values); 157.1-161.6°, 159.0° (6 values); S(cluster)-Fe-S(Ph), 100.4-123.4°, 113° (18 values); Mo-Fe-Fe, 60.2-61.5°, 60.8° (12 values); Fe-Fe-Fe, 59.0-61.2°, 60.0° (6 values); C-S, 1.75-1.81 Å, 1.77 (2) Å (8 values, disordered phenyl group excluded).

Here two chemically reversible reductions of the trianion ($i_{p,c}/i_{p,a} \simeq 1$ in CV) are observed together with a well-defined oxidation in DPP. Corresponding features occur in all other clusters of this type (Table IV). Peak half-widths of reduction and oxidation reactions are 100–120 mV, indicating by DPP criteria (90 mV for a reversible $n = 1$ transfer[26]) quasi-reversible one-electron processes. In certain clusters (e.g., R = p-C_6H_4Cl), two additional reductions have been observed at <−2 V by DPP[6] and may correspond to the processes 5−/6− and 6−/7−. Hence it appears that certain clusters (**1**) can give rise to the six-membered series (eq 1) in which each step corresponds to an electron-transfer reaction

$$\mathbf{1}: \; z = [2-] \leftrightarrow [3-] \rightleftharpoons [4-] \rightleftharpoons [5-] \leftrightarrow [6-] \leftrightarrow [7-] \quad (1)$$

of the subclusters of a given double-cubane cluster. The usual irreversibility of the 2−/3− reaction when examined by CV at relatively slow scan rates ($i_{p,a}/i_{p,c} \gg 1$, ≤ 100 mV/s) and the very negative potentials required for formation of the putative 6− and 7− clusters restrict feasible experimentation to the 3−, 4−, and 5− series members. The R = Ph system was selected for detailed

Table IV. DPP Peak Potentials of Mo-Fe-S Clusters in DMF Solution

cluster	E_p, V[e] (vs. SCE) 4−/5−	3−/4−	2−/3−
1, $[Mo_2Fe_6S_8(\mu_2\text{-}OMe)_3(S\text{-}t\text{-}Bu)_6]^{3-}$ [a]	−1.61	−1.40	−0.25[d]
2, $[Mo_2Fe_6S_8(SEt)_9]^{3-}$ [a]	−1.53	−1.32	−0.18
3, $[Mo_2Fe_6S_8(\mu_2\text{-}SEt)_3(SCH_2CH_2OH)_6]^{3-}$ [a]	−1.42	−1.22	−0.11
4, $[Mo_2Fe_6S_8(SCH_2Ph)_9]^{3-}$ [b]	−1.41	−1.19	−0.09
5, $[Mo_2Fe_6S_8(SCH_2CH_2OH)_9]^{3-}$ [a]	−1.37	−1.18	−0.10
6, $[Mo_2Fe_6S_8(S\text{-}p\text{-}C_6H_4OMe)_9]^{3-}$ [c]	−1.29	−1.08	−0.07
7, $[Mo_2Fe_6S_8(\mu_2\text{-}OMe)_3(SPh)_6]^{3-}$ [a]	−1.25	−1.05	+0.05
8, $[Mo_2Fe_6S_8(S\text{-}p\text{-}C_6H_4Me)_9]^{3-}$ [a]	−1.24	−1.06	−0.05
9, $[Mo_2Fe_6S_8(SPh)_9]^{3-}$ [c]	−1.23	−1.02	+0.01
10, $[Mo_2Fe_6S_8(S\text{-}p\text{-}C_6H_4Cl)_9]^{3-}$ [c]	−1.05	−0.85	+0.13
$[Mo_2Fe_6S_9(SEt)_8]^{3-}$ [a]	−1.56	−1.34	−0.18

[a] Et_4N^+ salt. [b] n-Pr_4N^+ salt. [c] n-Bu_4N^+ salt. [d] E_p(1−/2−) −0.03 V. [e] Measured at Pt electrode.

(26) Parry, E. P.; Osteryoung, R. A. *Anal. Chem.* **1965**, *37*, 1634.

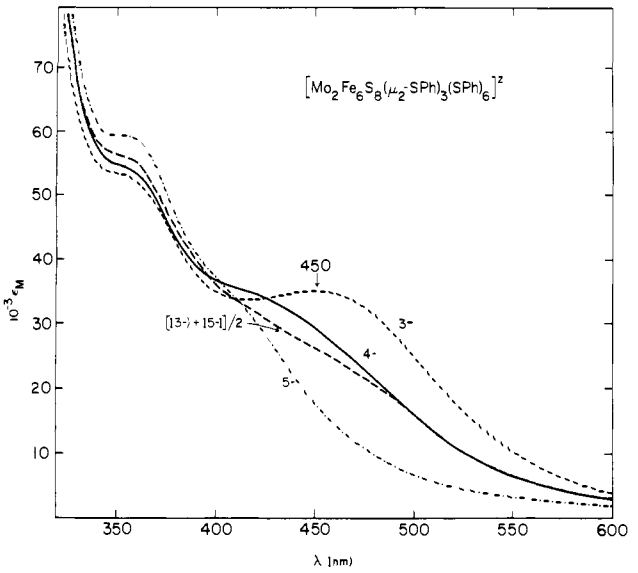

Figure 2. Absorption spectra of $[Mo_2Fe_6S_8(SPh)_9]^z$, z = 3–, 4–, 5–, in DMF solution; the 4– and 5– species were generated in an OTTLE cell at applied potentials of −1.13 and −1.43 V, respectively. Dashed line, calculated mean spectrum of 3– and 5– species.

study because its less negative potentials render the reduced clusters more stable to adventitious oxidation than those with R = alkyl.

Reaction 2 conducted with excess sodium acenaphthylenide

$$[Mo_2Fe_6S_8(SPh)_9]^{3-} \xrightarrow[MeCN/HMPA]{Na^+C_{12}H_8^-} [Mo_2Fe_6S_8(SPh)_9]^{5-} \quad (2)$$

yielded the 5– cluster, which was isolated as its crystalline Et_4N^+ salt. The structure of this cluster is described below. The 4– cluster is readily generated by the comproportionation reaction 3, for which $\log K_{com} = [E(3-/4-) - E(4-/5-)]/0.059$. In DMF

$$[Mo_2Fe_6S_8(SPh)_9]^{3-} + [Mo_2Fe_6S_8(SPh)_9]^{5-} \rightleftharpoons 2[Mo_2Fe_6S_8(SPh)_9]^{4-} \quad (3)$$

and DMA, $K_{com} = 10^{3.56}$, indicating essentially negligible concentrations of 3– and 5– species (mol fractions = 0.016 at equal initial concentrations) in solutions used for spectroscopic measurements. The 4– and 5– species have also been generated electrochemically in an OTTLE cell; absorption spectra are shown in Figure 2.

(b) $[Mo_2Fe_6S_8(\mu_2\text{-}OMe)_3(SR)_6]^z$ (2). In an attempt to investigate the oxidation reactions of type **1** clusters, the species $[Mo_2Fe_6S_8(S\text{-}t\text{-}Bu)_9]^{3-}$ was sought. On the basis of the R-substituent dependence of potentials in Table IV, the electron-releasing *tert*-butyl group is expected to shift all potentials to more negative values. Oxidation processes might then be observable at potentials well below that ($\gtrsim$+0.1 V) at which multielectron oxidation, a behavior common to all Mo–Fe–S clusters, occurs. The standard assembly reaction for type **1** clusters[2,5] afforded instead the methoxide-bridged double cubane **2**. Inasmuch as less-hindered

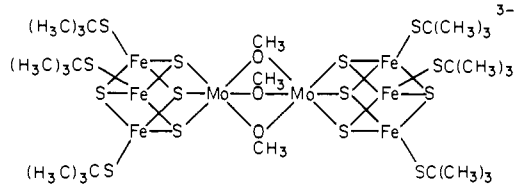

2

alkanethiolates in the same preparative system are thus far known to yield type **1** clusters only, it is probable that the expected cluster is destabilized by steric interactions among bridging and terminal substituents.[27] Formation of **2** reflects the pronounced tendency

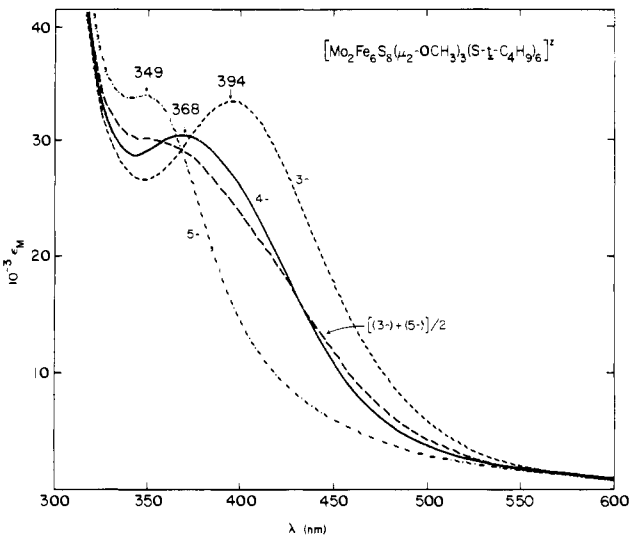

Figure 3. Absorption spectra of $[Mo_2Fe_6S_8(\mu_2\text{-}OMe)_3(S\text{-}t\text{-}Bu)_6]^z$, z = 3–, 4–, 5–, in DMF solution; the 4– and 5– species were generated in an OTTLE cell at applied potentials of −1.50 and −1.80 V, respectively. Dashed line, calculated mean spectrum of 3– and 5– species.

of the reaction system to form bridged clusters. Methoxide as such was not present in the system; the μ_2-OMe groups were derived from the methanol solvent. The species $[Mo_2Fe_6S_8(\mu_2\text{-}OMe)_3(SPh)_6]^{3-}$ has been prepared in the presence of *added* methoxide.[5] The structure of this cluster[5] is very similar to that of its tungsten analogue, for which crystallographic results, showing the presence of a $W(\mu_2\text{-}OMe)_3W$ bridge unit, have been published.[30] The Et_4N^+ salt of **2** was identified by elemental analysis, and bridging methoxide groups were demonstrated by ^1H NMR spectroscopy.[31]

As seen from the results in Figure 1, $[Mo_2Fe_6S_8(\mu_2\text{-}OMe)_3(S\text{-}t\text{-}Bu)_6]^{3-}$ undergoes two successive one-electron reductions and oxidations, defining the five-membered electron-transfer series (eq 4). When examined by CV (100 mV/s), these reactions are

$$\mathbf{2}: z = [1-] \rightleftharpoons [2-] \rightleftharpoons [3-] \rightleftharpoons [4-] \rightleftharpoons [5-] \quad (4)$$

chemically reversible. Potentials of the 2–/3– and 1–/2– processes (<0 V) reflect the inductive effect of *tert*-butyl substituents. Under the same experimental conditions, the 1–/2– step is not as well-defined in series based on $[Mo_2Fe_6S_8(\mu_2\text{-}OMe)_3(SPh)_6]^{3-}$ or for a number of type **1** clusters. Series 4 demonstrates the existence of double-cubane species whose subclusters exist in the core oxidation levels $[MoFe_3S_4]^{2+,3+,4+}$. For the various types of Mo–Fe–S clusters,[2-6] this is the most extensive series consisting of demonstrably reversible steps. However, over the times required for chemical or electrochemical oxidation, isolation, and purification, we have not yet been able to obtain analytically pure specimens of 1– or 2– cluster salts. Reduced clusters are readily generated electrochemically; their absorption spectra are presented in Figure 3. These and other spectra of reduced clusters are additionally considered in a following section.

(27) The $Mo(\mu_2\text{-}S\text{-}t\text{-}Bu)_3Mo$ bridge unit does occur in $Mo_2(CO)_2L(S\text{-}t\text{-}Bu)_3(\eta^7\text{-}C_7H_7)$ (L = $P(OMe)_3$,[28a] CO[28b]). In these molecules steric interactions of bridge and terminal ligands may be less unfavorable than in **2**, and additional stabilization presumably derives from a metal–metal bond (Mo–Mo ~2.9 Å). In type **1** clusters the latter feature is absent (Mo–Mo ~3.7 Å[2,7,8,29]).

(28) (a) Benson, I. B.; Knox, S. A. R.; Naish, P. J.; Welch, A. J. *J. Chem. Soc., Chem. Commun.* **1978**, 878. (b) Weidenhammer, K.; Ziegler, M. L. *Z. Anorg. Allg. Chem.* **1979**, *458*, 29.

(29) Christou, G.; Garner, C. D.; Mabbs, F. E.; Drew, M. G. B. *J. Chem. Soc., Chem. Commun.* **1979**, 91.

(30) Christou, G.; Garner, C. D.; King, T. J.; Johnson, C. E.; Rush, J. D. *J. Chem. Soc., Chem. Commun.* **1979**, 503.

(31) The OMe shift of +3.07 ppm (Experimental Section) compares with ~+3 ppm (broad signal) for $[Mo_2Fe_6S_8(\mu_2\text{-}OMe)_3(SPh)_6]^{3-}$, whose ^1H NMR[5] and electrochemical[6] properties are very similar to those of $[W_2Fe_6S_8(\mu_2\text{-}OMe)_3(SPh)_6]^{3-}$.

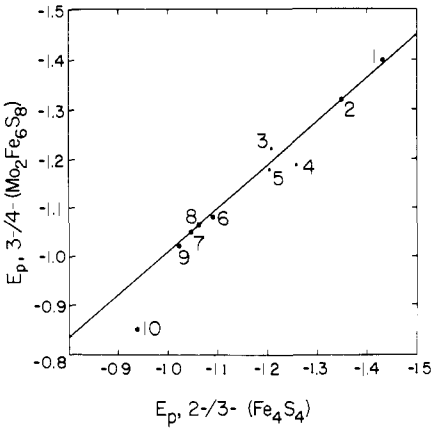

Figure 4. Plot illustrating correlation of 3−/4− potentials of clusters 1–10 in Table IV with E_p values of $[Fe_4S_4(SR)_4]^{2-,3-}$ couples in DMF. The line is a fit to all data points except 3 and 10.[34]

(c) Redox Potentials. An apparent regularity of $[Mo_2Fe_6S_8(SR)_9]^{3-,4-}$ potentials, from three sets of comparative data already published,[6] is their parallel behavior with potentials of the reversible $[Fe_4S_4(SR)_4]^{2-,3-}$ couples upon variation of the substituent R. This behavior has been examined more fully by the use of seven sets of data which include clusters 2, 4, 5, 6, 8–10 in Table IV and the correspondingly substituted Fe–S clusters.[32] These data, plotted in Figure 4, were fit by linear regression analysis to eq 5 (determination coefficient $r^2 = 0.97$). Excluded is the obviously

$$E_p(\text{MoFeS}) = 0.85E_p(\text{FeS}) - 0.16 \quad (5)$$

deviant point 10 (R = p-C_6H_4Cl), which may be representative of the behavior of an uninvestigated set of clusters with conjugative phenyl group substituents. Not only do the measured potentials reveal an essentially linear correlation but their values in the two series of clusters differ by only 70 mV (R = CH_2Ph) and ≤30 mV for other cases (excluding 10). Inasmuch as $[Fe_4S_4(SR)_4]^{2-,3-}$ and the subclusters of $[Mo_2Fe_6S_8(SR)_9]^{3-,4-}$ do not have the same net or core charges and are not isoelectronic, there is no a priori reason why their potentials should be so similar. We concur with an earlier observation[6] that this similarity is a consequence of addition and removal of electrons from subcluster orbitals, which in the two cases are of appreciable Fe–S character[34] and whose energies are shifted nearly linearly by variation of R. The first of these contentions is supported by the Mössbauer spectral results below.

Structure of $[Mo_2Fe_6S_8(SPh)_9]^{5-}$. The most immediate result of the crystallographic investigation is verification of the retention of the double-cubane structure in the two-electron reduction product of reaction 2. This compound, $(Et_4N)_5[Mo_2Fe_6S_8(SPh)_9]$, crystallizes in monoclinic space group $P2_1/c$ and consists of well-separated cations and anions. Crystal data are contained in Table I. Structural properties of ordered cations and benzenethiolate ligands are unexceptional and are not considered. The structural features of the entire anion and of its individual $MoFe_3S_4(SPh)_3$ clusters are quite comparable to those described at some length for $[Mo_2Fe_6S_8(SEt)_9]^{3-}$ [2] and other species containing the same type of subcluster.[10-12] Because a corresponding structural description for $[Mo_2Fe_6S_8(SPh)_9]^{5-}$ readily follows from the depiction of the anion in Figure 5 and the metrical data in Table III and supplemental tables, salient structural features are only briefly noted. (1) No crystallographic symmetry is imposed on the anion, which (excluding benzenethiolate ligands) approaches D_{3h} symmetry. (2) The cubane-type $MoFe_3S_4$ core units of the subclusters consist of two interpenetrating, imperfect, and nearly concentric tetrahedra ($MoFe_3$, S_4), of which S_4 has the larger volume. (3) The $MoFeS_2$ and Fe_2S_2 core faces are decidedly nonplanar rhombs; core diagonal planes ($MoFeS_2$, Fe_2S_2) are more nearly perfect. (4) Core units are dominantly trigonally distorted (idealized C_{3v} symmetry), a property reflected in two ranges of Fe–S distances: Fe–S (4, 14), 2.288–2.322 Å, mean 2.305 (12) Å; others, 2.253–2.281 Å, mean 2.271 (8) Å.

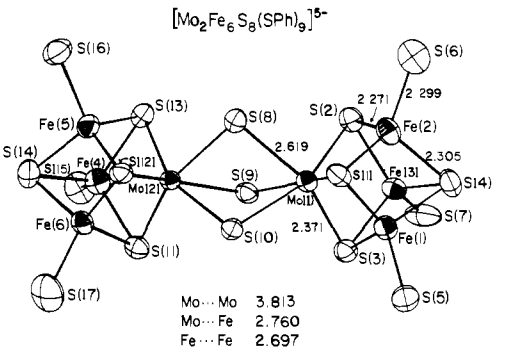

Figure 5. Structure of $[Mo_2Fe_6S_8(SPh)_9]^{5-}$, showing 50% probability ellipsoids, the atom labeling scheme, and selected mean interatomic distances; not included are the nine phenyl rings of the bridging and terminal thiolate ligands.

Table V. Comparison of Mean Values of Selected Structural Features of $[Mo_2Fe_6S_8(SR)_9]^z$ Clusters

feature[a]	$[Mo_2Fe_6S_8(SPh)_9]^{5-}$ [b]	$[Mo_2Fe_6S_8(SEt)_9]^{3-}$ [c]	$[Mo_2Fe_6S_8(SPh)_9]^{3-}$ [d]
$Mo(\mu_2\text{-}SR)_3Mo$			
Mo···Mo	3.813 (2)	3.668 (4)	3.685 (3)
Mo–S	2.619 (23)	2.567 (4)	2.58 (2)
Mo–S–Mo	93.5	91.2 (2)	[e]
$MoFe_3S_4(SR)_3$			
Mo–S	2.371 (11)	2.351 (3)	2.34 (2)
Mo···Fe	2.760 (14)	2.723 (2)	2.71 (2)
Fe–S	2.282 (19)	2.260 (10)	2.25 (3)
Fe–SR	2.299 (11)	2.232 (5)	2.25 (3)
$V(MoFe_3)$	2.39	2.33	
$V(S_4)$	5.74	5.59	[f]
$V(MoFe_3S_4)$	9.62	9.37	

[a] Distances, Å; angles, deg; volumes, Å^3. [b] This work. [c] Reference 2. [d] Reference 7. [e] Not reported. [f] Insufficient data for volume calculations.

Particular interest attends cluster dimensional changes upon reduction, a matter examined with the aid of the comparative structural data in Table V. The structure of $(Et_3NCH_2Ph)_3[Mo_2Fe_6S_8(SEt)_9]^2$ (R = 4.8%) is the most accurate currently available for a $[Mo_2Fe_6S_8(SR)_9]^{3-}$ (**1**) cluster. Because of the identity of R substituents the less-refined structure of $(n\text{-}Bu_4N)_3[Mo_2Fe_6S_8(SPh)_9]^7$ (R = 8.8%) is included in Table V. However, the slight structural differences among $[Mo_2Fe_6S_8(SR)_9]^{3-}$ clusters with variant R groups and countercations, apparent in some four structures at their present stages of refinement,[2,7,8,29] are smaller than differences between 3– and 5– clusters. Distances in the reduced cluster tend to be longer. In addition, the nonbonded Mo···S distances in the subclusters are greater in $[Mo_2Fe_6S_8(SPh)_9]^{5-}$ (3.976 (4), 3.980 (4) Å) than in $[Mo_2Fe_6S_8(SEt)_9]^{3-}$ (3.899 (7) Å[2]). These distance differences result in larger $MoFe_3$, S_4, and core $MoFe_3S_4$ volumes in the reduced cluster. The core mean volume increase of 2.6% upon the one-electron reductions of the subclusters may be compared to values for Fe_4S_4 volume increases in the pairs $[Fe_4S_4(SR)_4]^{2-/3-}$: 1.9% (R = Ph[23,25]), 2.7% (R = CH_2Ph[15,35]). Unlike these cases,

(32) $[Fe_4S_4(SR)_4]^{2-,3-}$ potentials are not tabulated, for they are closely similar to $E_{1/2}$ values already reported.[17,19,33]

(33) DePamphilis, B. V.; Averill, B. A.; Herskovitz, T.; Que, L., Jr.; Holm, R. H. *J. Am. Chem. Soc.* **1974**, *96*, 4159.

(34) Indeed, variation of the bridging group $(\mu_2\text{-}SR)_3 \rightarrow (\mu_2\text{-}OMe)_3$ with terminal R substituents constant has only a small effect on potentials (Table IV). Inclusion of the data of clusters 1 and 7 and the correspondingly substituted Fe–S clusters in a linear fit alters eq 5 only slightly, to $E_p(\text{MoFeS}) = 0.87(\text{FeS}) - 0.14$ ($r^2 = 0.98$). This line is plotted in Figure 4. A linear behavior also obtains for $[Mo_2Fe_6S_8(SR)_9]^{4-,5-}$ potentials, which exhibit a nearly constant difference (mean value 0.20 (1) V) from 3–/4– potentials.

(35) Berg, J. M.; Hodgson, K. O.; Holm, R. H. *J. Am. Chem. Soc.* **1979**, *101*, 4586.

however, bond distance alterations are not largely localized in particular bonds, thereby leading to recognizable changes from one sort of idealized core geometry to another.[23,35] Instead, bonded and nonbonded distance changes appear to be distributed throughout the cores. Structural feature 4 of the reduced cluster also occurs in $[Mo_2Fe_6S_8(SEt)_9]^{3-}$. The substantial increase ($\sim$ 0.07 Å) in Fe–SR distances demonstrates that the added electrons diminish the Fe(III) character of the cores,[36] consistent with Mössbauer spectral results (vide infra). Increases of 0.03–0.05 Å in Fe–SR bond distances are found in the aforementioned Fe–S cluster pairs,[15,23,25,35] in which the mean oxidation state change $Fe^{2.5+} \rightarrow Fe^{2.25+}$ occurs upon reduction. Lastly, the $\sim$0.14-Å increase in Mo···Mo separation probably is mainly a consequence of decreased positive charge at the Mo sites as each core charge is reduced by one unit. Such an effect would decrease the electrostatic component of Mo–SR^- (bridge) bonding interactions. If core–core overall charge repulsions were dominant and terminal–bridge ligand interactions were constant, a decrease in Mo···Mo separation in the reduced form would be anticipated.

Electronic Structural Properties of Clusters. For species as complex as **1** and its reduced forms, an ultimately satisfactory electronic structural description will require theoretical calculations of energy levels and orbitals that accord with measured properties. Our earlier investigation of electronic structures[2,3,37] was confined to the 3– clusters of series 1 and led to an electronic structural proposal in terms of Fe and Mo oxidation states. This is given in series 6, which contains those oxidation levels in series 1 that

$$\mathbf{1}: \quad [(2\alpha)]^{3-} \rightleftharpoons [(\alpha + \beta)]^{4-} \rightleftharpoons [(2\beta)]^{5-} \qquad (6)$$

$$\alpha = [Mo^{3+}Fe_3^{2.67+}S_4^{2-}]^{3+}; \ \beta = [Mo^{3+}Fe_3^{2.33+}S_4^{2-}]^{2-}$$

have been studied in this work. Charge distributions are represented by α and β; the superscripted oxidation state of iron is the mean value of the states of the three Fe atoms. The generation of the 4– and 5– members of the series, together with the isolation and structure proof of $[Mo_2Fe_6S_8(SPh)_9]^{5-}$, has permitted widening of the electronic structural investigation to these species. In the following sections certain spectroscopic and magnetic properties of reduced clusters are detailed and interpreted in terms of two key features: electron distribution within $MoFe_3S_4$ subclusters as dependent on oxidation level of a double-cubane entity; electron delocalization between subclusters in cases where they do not necessarily have equivalent oxidation levels. Recently the Manchester/Liverpool groups (ML) have reported spectroscopic and magnetic properties of the double cubanes $[Mo_2Fe_6S_8(SR)_9]^{3-}$ and $[Mo_2Fe_6S_8(\mu_2\text{-}OMe)_3(SR)_6]^{3-}$.[5,6,38] This work, which does not include reduced clusters, is complementary to our prior and present investigations. Where direct comparisons can be made, experimental results are in adequate agreement; however, certain conclusions concerning electron distribution differ.

(a) Electronic Spectra. A spectroelectrochemical technique with an OTTLE cell was employed to obtain the spectra of reduced clusters. Spectra of the 3–, 4–, and 5– members of series 1 and 4 are compared in Figures 2 and 3. In each series, the 4– species was generated at the exact potential of minimum current between 3–/4– and 4–/5– steps in the DP polarogram (cf. Figure 1). Spectral changes in DMF solutions proved to be reversible. Typicaly, the reduction–oxidation cycle [3–] → [4–] → [5–] → [4–] → [3–] performed over a period of $\sim$5 h recovered the original spectrum of the 3– cluster with a 5–7% intensity loss at λ_{max}. The spectra shown are those obtained in the initial reductions. The spectrum of generated $[Mo_2Fe_6S_8(SPh)_9]^{5-}$ is identical with that of its isolated Et_4N^+ salt. All spectra, including those of $[Mo_2Fe_6S_8(SEt)_9]^{3-,4-,5-}$ (λ_{max} 394 (3–), 374 (4–), 355 nm (5–); not shown), exhibit blue shifts of band maxima or shoulders upon reduction. The series in Figure 3, for example,

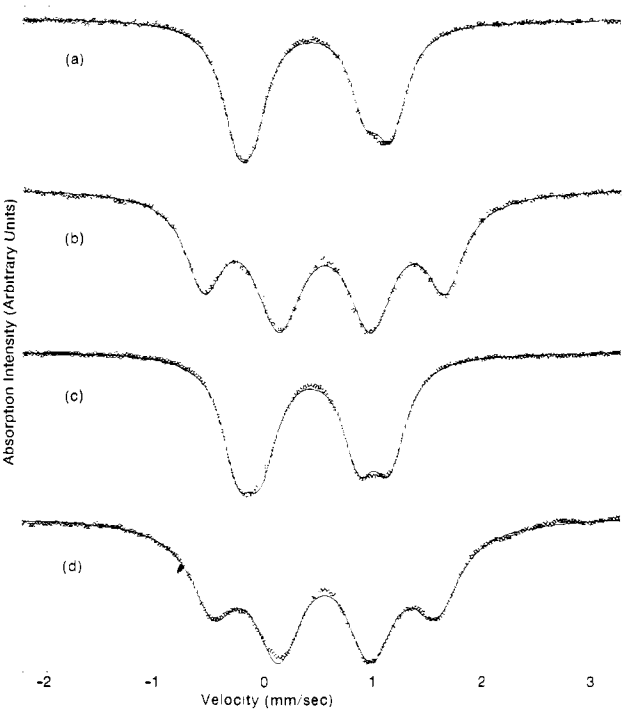

Figure 6. Mössbauer spectra at 4.2 K: (a) $(n\text{-}Bu_4N)_3[Mo_2Fe_6S_8(SPh)_9]$, solid; (b) $(Et_4N)_5[Mo_2Fe_6S_8(SPh)_9]$, solid; (c) $[Mo_2Fe_6S_8(SPh)_9]^{3-}$, $\sim$1 mM DMA solution; (d) $[Mo_2Fe_6S_8(SPh)_9]^{5-}$, $\sim$1 mM DMA solution. The solid lines are theoretical fits of the spectra using the parameters in Table VI.

shows the changes 394 (3–), 368 (4–), 349 nm (5–). This is the behavior expected for terminal-RS → core charge transfer inasmuch as displacements to higher energies should occur as core oxidation level is decreased. Analogous behavior is observed in the spectra of $[Fe_4S_4(SR)_4]^{2-,3-}$ clusters,[39] where this type of transition is fairly well established.

Spectra of $[Mo_2Fe_6S_8(SPh)_9]^{4-}$ and $[Mo_2Fe_6S_8(\mu_2\text{-}OMe)_3(S\text{-}t\text{-}Bu)_6]^{4-}$ are pertinent to the existence of subcluster mixed-oxidation levels (α, β), but at a time scale $\gtrsim 10^6$ shorter than that of Mössbauer spectroscopy (vide infra). In Figures 2 and 3, spectra of these 4– clusters are compared to those calculated from the average of 3– and 5– cluster spectra. The latter are the spectra which should obtain if the subclusters act as independent, inequivalent chromophores. Although band shapes are clearly similar, exact matches between observed and calculated spectra are not found.[40] In particular, the observed 4– cluster spectrum in Figure 3 has a maximum at 368 nm not present in the average spectrum. While close inspection of the 4– cluster spectra could lead to the conclusion that, from the average spectra, the systems contain contributions from unreduced 3– species as a result of incomplete electrolysis, this is unlikely to be the case. The spectrum of $[Mo_2Fe_6S_8(SPh)_9]^{4-}$ in Figure 2 is indistinguishable from that of the product of reaction 3 in DMA solution.[14] We conclude that the spectra of this cluster and $[Mo_2Fe_6S_8(\mu_2\text{-}OMe)_3(S\text{-}t\text{-}Bu)_6]^{4-}$ correspond to species with inequivalent subcluster chromophores, which, evidently, are not strictly independent. The same conclusion applies to $[Mo_2Fe_6S_8(SEt)_9]^{4-}$.

(b) Mössbauer Spectra. The clusters $[Mo_2Fe_6S_8(SPh)_9]^{3-,4-,5-}$ of series 6 have been examined in the solid state (3–, 5–) and in DMA solutions (3–, 4–, 5–) from 4.2 K to temperatures up to 180 K in several cases. Only results obtained in the absence of an applied magnetic field are considered. These spectra, presented in Figures 6–8, usually consist of overlapping quadrupole doublets. Theoretical fits of all 3– and 5– cluster spectra have been made

(36) The effective ionic radius difference $r(Fe(II)) - r(Fe(III)) \simeq 0.14$ Å: Shannon, R. D. *Acta Crystallogr., Sect. A* **1976**, *A32*, 751.
(37) Frankel, R. B.; Wolff, T. E.; Power, P. P.; Holm, R. H. *J. Phys. (Paris)* **1980**, *41*, C1-495.
(38) Christou, G.; Collison, D.; Garner, C. D.; Mabbs, F. E.; Petrouleas, V. *Inorg. Nucl. Chem. Lett.* **1981**, *17*, 137.
(39) Cambray, J.; Lane, R. W.; Wedd, A. G.; Johnson, R. W.; Holm, R. H. *Inorg. Chem.* **1977**, *16*, 2565.
(40) Intensity deviations of observed from calculated spectra, amounting to +(8–12)% at 420–450 nm and –10 to +9% at 340–450 nm, occur in Figures 2 and 3, respectively.

Table VI. Mössbauer Spectral Data for Mo-Fe-S Clusters

	T, K	mm/s δ_1[a,b]	ΔE_{Q_1}[b]	δ_2[a,b]	ΔE_{Q_2}[b]	Γ_1[c]	Γ_2[c]	A_1,[d] %	A_2,[d] %
				$[Mo_2Fe_6S_8(SPh)_9]^{3-}$					
solid[e]	4.2	0.28	1.01	0.32	1.41	0.31	0.35	38	62
	80	0.28	0.99	0.31	1.37	0.32	0.30	63	37
	130	0.26	0.95	0.29	1.28	0.32	0.31	61	39
	180	0.25	0.89	0.38	1.15	0.28	0.30	44	56
DMA solution	4.2	0.29	0.91	0.32	1.41	0.38	0.35	53	47
	80	0.28	0.85	0.30	1.26	0.36	0.31	64	36
	130	0.27	0.79	0.28	1.14	0.34	0.30	61	39
	180	0.25	0.73	0.25	1.04	0.32	0.30	49	51
				$[Mo_2Fe_6S_8(SPh)_9]^{5-}$					
solid[e]	4.2	0.42	0.84	0.41	2.21	0.54	0.42	65	35
	80	0.41	0.85	0.40	1.94	0.56	0.45	76	24
	130	0.39	0.79	0.38	1.56	0.56	0.59	66	34
DMA solution[f]	4.2	0.43	0.85	0.42	2.05	0.54	0.52	62	38
	80	0.39	0.82	0.40	1.91	0.48	0.42	69	31
	130	0.37	0.78	0.39	1.76	0.48	0.44	70	30
				$[Mo_2Fe_6S_8(SPh)_9]^{4-}$					
DMA solution, 4-site fit, unconstrained parameters[g]	80	0.27	0.77	0.32	1.21	0.29	0.46	20	44
		0.41	0.75	0.39[b]	2.10[b]	0.31	0.34	24	12
4-site fit, constrained intensities[g]	80	0.32[g]	0.99[g]	0.32	1.31	0.40	0.38	35	15
		0.35[g]	0.69[g]	0.39[b]	2.07[b]	0.39	0.39	33	17
				DMA solution					
$[Mo_2Fe_6S_8(SEt)_9]^{3-}$	4.2	0.29	0.99	0.32	1.50	0.39	0.43	53	47
$[Mo_2Fe_6S_9(SEt)_8]^{3-}$	4.2	0.30	1.01	0.33	1.49	0.38	0.40	53	47
$[Mo_2Fe_6S_9(SEt)_8]^{5-}$	4.2	0.44	0.99	0.45	2.18	0.52	0.40	71	29

[a] Relative to Fe metal at 4.2 K. Subscripts on this and other symbols refer to sites 1 and 2 of a subcluster. [b] Estimated uncertainties are ±0.02 mm/s in δ and ±0.04 mm/s in ΔE_Q unless noted otherwise. [c] Linewidths at half-maximum intensity. [d] Relative absorptions, ±10%. [e] Et_4N^+ salt. [f] An impurity spectrum corresponding to ~18% of the total absorption at the indicated temperatures was subtracted prior to spectral analysis. No impurity was present in spectra of the isolated Et_4N^+ salt. [g] Estimated uncertainties are ±0.04 mm/s in δ and ±0.08 mm/s in ΔE_Q except for values noted as *b*.

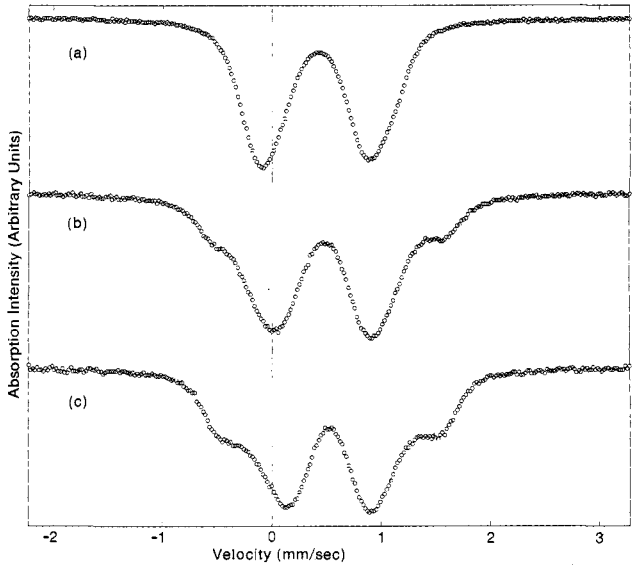

Figure 7. Mössbauer spectra of ~1 mM DMA solutions at 80 K: (a) $[Mo_2Fe_6S_8(SPh)_9]^{3-}$; (b) $[Mo_2Fe_6S_8(SPh)_9]^{4-}$; (c) $[Mo_2Fe_6S_8(SPh)_9]^{5-}$.

on the basis of two quadrupole doublets with Lorentzian line shapes. Spectral parameters from the computer fits are collected in Table VI. The spectra of $[Mo_2Fe_6S_8(SPh)_9]^{3-}$ in the solid and in frozen solutions (Figure 6) differ insignificantly, indicating no important structural or electronic differences in the two phases. These spectra resemble that of polycrystalline $(Et_4N)_3[Mo_2Fe_6S_8(SEt)_9]$, whose crystal structure at ambient temperature[2] provides no evidence of the inequivalence of Fe sites reflected in the low-temperature Mössbauer spectrum. These same observations apply to solid and solution spectra of $[Mo_2Fe_6S_8(SPh)_9]^{5-}$, but with additional comments. Two quadrupole doublets of ~2:1 intensity ratio are clearly resolved at 4.2 K in solid and solution spectra (Figure 6). Isomer shifts (0.41–0.43 mm/s) are scarcely different for these doublets, with the less intense doublet associated with the larger quadrupole splitting. Inasmuch as all Fe sites in crystalline $(Et_4N)_5[Mo_2Fe_6S_8(SPh)_9]$ are inequivalent, the appearance of more than one doublet is not unexpected. However, the difference in quadrupole splittings between the two types of sites is substantially larger ($\gtrsim$1 mm/s) than in the 3– cluster ($\lesssim$0.4 mm/s). Other than noting that all Fe sites are crystallographically equivalent in $[Mo_2Fe_6S_8(SEt)_9]^{3-}$, we are unable to identify clearly a structural basis for the larger difference from the ambient-temperature crystal structure of the reduced cluster. Because the population ratio of the two types of Fe sites in the latter is distinctly not unity at all temperatures up to 130 K, these sites are associated with a 1:2 distribution within subclusters rather than arising from inequivalent subclusters. It is emphasized that this distribution applies in frozen solution (Table VI), where environmental influences on cluster geometry and site inequivalencies should be minimized.[41]

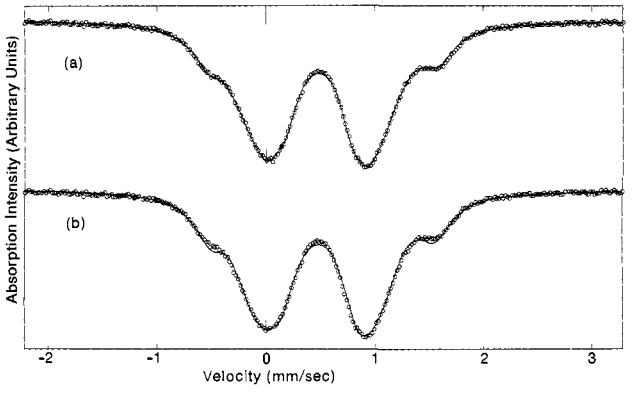

Figure 8. Mössbauer spectra of ~1 mM $[Mo_2Fe_6S_8(SPh)_9]^{4-}$ in DMA at 80 K: (a) four-site fit with all parameters unconstrained; (b) four-site fit with localized cluster oxidation levels $\alpha + \beta$, each constrained to 50% of the total absorption intensity and 1:2 relative intensities of sites in subclusters. The parameters for these fits are given in Table VI.

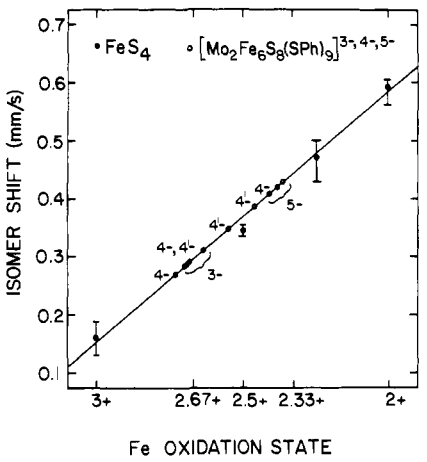

Figure 9. Dependence of ^{57}Fe isomer shifts at 4.2 K (vs. Fe metal at 4.2 K) in tetrahedral FeS_4 sites (●) on the mean oxidation state of the metal. Bars indicate ranges of values and points are average values. Isomer shifts of Mo–Fe–S clusters in solid and solution (○, Table VI) are extrapolated to the line, which is a fit of the FeS_4 data by linear regression analysis. All cluster values were determined at 4.2 K except those of $[Mo_2Fe_6S_8(SPh)_9]^{4-}$, which derive from spectral fits of the 80-K solution spectrum. Unprimed (4–) and primed (4′–) isomer shifts of this cluster refer to fits with unconstrained parameters and constrained relative intensities, respectively (see text).

Reduction of $[Mo_2Fe_6S_8(SPh)_9]^{3-}$ to the 5– oxidation level results in isomer shift increases of 0.09–0.14 and 0.10–0.14 mm/s at 4.2 K in the solid and solution states, respectively. These changes signify a decrease in the oxidation state of the Fe atoms, a matter interpreted by means of the plot in Figure 9. Here isomer shifts δ of Fe atoms in tetrahedral FeS_4 sites at 4.2 K are observed to vary nearly linearly with mean oxidation state s and have been fitted to eq 7 ($r^2 = 1.00$). All values of δ refer to

$$\delta = 1.44 - 0.43s \qquad (7)$$

well-characterized Fe–S complexes[23,24,42-46] and, in the interest of experimental uniformity, have been drawn from measurements in this laboratory only. The shifts of $[Mo_2Fe_6S_8(SPh)_9]^{3-}$ at 4.2 K give $s = 2.60$–2.70, indicating the mean oxidation state description $Fe^{2.67+}$, as obtained for $[Mo_2Fe_6S_8(SEt)_9]^{3-}$ by a similar procedure.[2] Subsequent to our introduction of the δ/s plot,[2] the electronically delocalized cluster $[Fe_6S_9(S\text{-}t\text{-}Bu)_2]^{4-}$ has been prepared.[46] It is the only discrete Fe–S species with tetrahedral sites for which, necessarily, $s = 2.67$. Its isomer shifts (0.28–0.29 mm/s, 4.2 K) agree reasonably well with those of the 3– clusters. Isomer shifts of $[Mo_2Fe_6S_8(SPh)_9]^{5-}$ at 4.2 K afford $s = 2.35$–2.40 from eq 7. These results demonstrate that the electrons added in reduction of the 3– species have appreciable Fe orbital character in the 5– cluster.

Spectra of the intermediate member of series 6, $[Mo_2Fe_6S_8(SPh)_9]^{4-}$, generated in DMA solution by reaction 3, are complicated at 4.2 K by magnetic hyperfine interactions due to slow electron spin relaxation. This situation is avoided at higher temperatures. The 80-K spectrum, compared in Figure 7 with those of the 3– and 5– clusters under the same conditions, consists of an intense, broadened central doublet flanked by a less intense doublet with a comparable isomer shift but a larger quadrupole splitting. The spectrum resembles a near superposition of the 3– and 5– cluster spectra, a possibility examined by computer fitting trials. The most satisfactory fits to the experimental spectrum at 80 K are those presented in Figure 8. Both fits incorporate the twofold site inequivalencies in the subclusters of 3– and 5– species already noted in their 4.2-K spectra (Figure 6). Persistence of inequivalencies in solution at 80 K is visually apparent from the broadened quadrupole doublet (3–) and partially resolved doublet of doublets (5–) in Figure 7. In spectrum a of Figure 8, the centroids, splittings, line widths, and relative intensities of the four doublets were left as unconstrained parameters. In spectrum b, the relative intensities of the four doublets were constrained to be very near 2:1/2:1, based on the site 1:site 2 ratios of ~2:1 found from fits of the 3– and 5– cluster solution spectra at 80 K. All other parameters were unconstrained. The parameters obtained from both models are compiled in Table VI. The unconstrained model does not afford a 1:1 absorption ratio of subclusters and therewith presents a departure from the 2:1/2:1 intensity ratio of their inequivalent sites. The values of the free parameters in both models are close enough to those of 3– and 5– cluster spectra to maintain the validity of the approach.

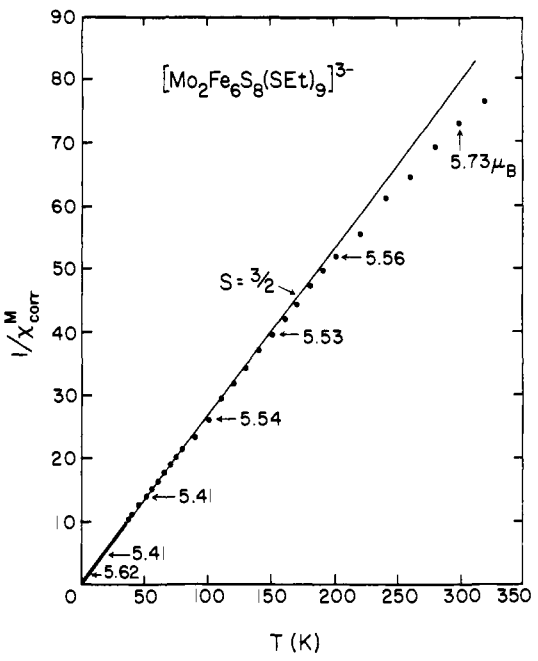

Figure 10. Temperature dependence of the reciprocal of the magnetic susceptibility of $(Et_3NCH_2Ph)_3[Mo_2Fe_6S_8(SEt)_9]$. Values of magnetic moments at various temperatures calculated from the Curie law μ (μ_B) $= 2.829(\chi_M T)^{1/2}$ are given; the magnetic moment per subcluster $= \mu/2^{1/2}$. The line corresponds to Curie behavior of two noninteracting $S = {}^3/_2$ spin systems.

Isomer shifts of the 3–, 4–, and 5– species have been extrapolated to the line of eq 7 in Figure 9. Except for $\delta_1 = 0.35$ mm/s and $\delta_2 = 0.39$ mm/s from the intensity-constrained fit of the 4– cluster spectra, the values for the 4– species fall in the regions of 3– and 5– cluster values. The preceding two values do, however, indicate a more reduced set of Fe atoms in one subcluster than in the other. From the collective Mössbauer spectral results we conclude that $[Mo_2Fe_6S_8(SPh)_9]^{4-}$ contains inequivalent subclusters ($\alpha + \beta$) with Fe mean oxidation states the same as those in the equivalent subclusters (2α,2β) of $[Mo_2Fe_6S_8(SPh)_9]^{3-,5-}$. These conclusions are presented in series 6; other comments concerning oxidation state assignments are given below. By Mössbauer spectral criteria, $[Mo_2Fe_6S_8(SPh)_9]^{4-}$ is a "mixed" subcluster species, with the rate constant for intramolecular electron transfer ($k \lesssim 7 \times 10^6$ s^{-1}) slower than the rate of ^{57}Fe excited nuclear state decay at $T \leq 80$ K.

(c) Magnetism. The temperature dependence of the magnetic susceptibility χ^M of polycrystalline $(Et_3NCH_2Ph)_3[Mo_2Fe_6S_8(SEt)_9]$ is shown in Figure 10. This compound exhibits a near

(41) Structural changes between crystalline and frozen solution states as manifested by Mössbauer spectra have been observed for other reduced clusters, viz., $[Fe_4S_4(SR)_4]^{3-}$.[23,42]

(42) Laskowski, E. J.; Reynolds, J. G.; Frankel, R. B.; Foner, S.; Papaefthymiou, G. C.; Holm, R. H. *J. Am. Chem. Soc.* **1979**, *101*, 6562.
(43) Lane, R. W.; Ibers, J. A.; Frankel, R. B.; Papaefthymiou, G. C.; Holm, R. H. *J. Am. Chem. Soc.* **1977**, *99*, 84.
(44) Frankel, R. B.; Papaefthymiou, G. C.; Lane, R. W.; Holm, R. H. *J. Phys. (Paris)* **1976**, *37*, C6-165.
(45) Frankel, R. B.; Averill, B. A.; Holm, R. H. *J. Phys. (Paris)* **1974**, *35*, C6-107.
(46) Christou, G.; Holm, R. H.; Sabat, M.; Ibers, J. A. *J. Am. Chem. Soc.* **1981**, *103*, 6269.

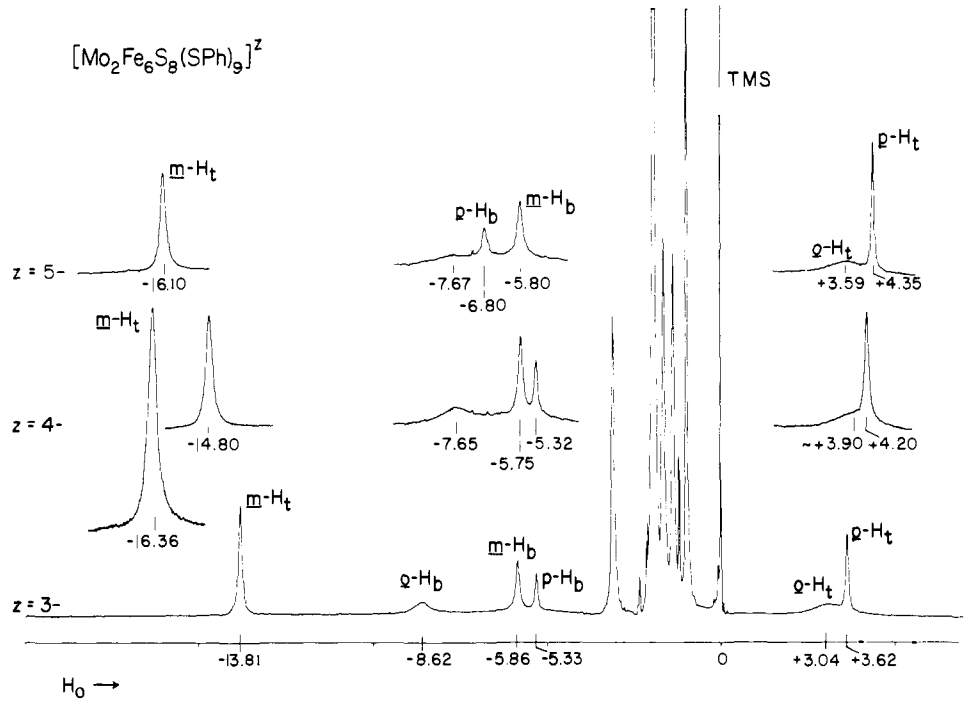

Figure 11. ^1H NMR spectra of $[Mo_2Fe_6S_8(SPh)_9]^z$ in CD_3CN solutions at 296K, illustrating variation of chemical shifts with oxidation level. Signal assignments (t = terminal, b = bridging ligand) are indicated; those for the $z = 5-$ spectrum apply to the $z = 4-$ spectrum. The inset in the latter spectrum is the m-H_t resonance at 238 K. The 4- cluster was generated by reaction 3 by using equimolar amounts of reactants. Signals of n-Bu_4N^+ and protio solvent are unlabeled.

dependence on the Curie law at 4.2–150 K, indicating that energy separations between any spin manifold states arising from spin coupling within and between subclusters are small or large compared to kT over this temperature interval. While several interpretations of these results are conceivable (including that advanced for the magnetic properties of $(Et_4N)_3[Mo_2Fe_6S_8(\mu_2\text{-}OMe)_3(SPh)_6]$[38]), we currently favor assignment of a $S = {}^3/_2$ ground state to subclusters with weak or negligible spin coupling between them at $T > 4.2$ K. This assignment is consistent with spin-quartet EPR spectra observed at 7 K for magnetically isolated clusters having the α core oxidation level and magnetic moments $\mu = \sim 4.0\ \mu_B$ in solution at 298 K.[12] Increasing deviation from linear behavior above 150 K presumably is due to population of subcluster spin states of higher multiplicity.

Magnetic moments of $[Mo_2Fe_6S_8(SPh)_9]^{3-,4-,5-}$ in acetonitrile solutions at 296 K are given in Table VII. The value for the 3- cluster is in good agreement with that (5.70 μ_B) in Me_2SO solution at the same temperature.[5]. The finding that $[(\mu^2(3-) + \mu^2(5-))/2]^{1/2} = 6.28\ \mu_B$ is within experimental error of $\mu(4-) = 6.24\ \mu_B$ supports the proposal that the 4- cluster contains the $\alpha + \beta$ subclusters present separately in the 3- and 5- species and that their interaction energies are $<kT$. The magnetic moments of the 3-, 4-, and 5- clusters are very close to the spin-only values predicted for two $S = {}^3/_2$ (5.47 μ_B), one $S = {}^3/_2$ and one $S = 2$ (6.23 μ_B), and two $S = 2$ (6.90 μ_B) subclusters, respectively. Both the solid state and solution data show that subcluster metal spins are coupled, as is the case in $[Fe_4S_4(SR)_4]^{2-,3-}$ species.[23,42,47] Further discussion of ground-state spin properties will be deferred until completion of an investigation of magnetically perturbed Mössbauer spectra.[47]

(d) ^1H NMR Spectra. Shown in Figure 11 are 300-MHz spectra of $[Mo_2Fe_6S_8(SPh)_9]^{3-,4-,5-}$ in acetonitrile solutions at 296 K. The isotropic shifts of terminal and bridging substituents in the 3- case arise predominantly from contact and dipolar mechanisms, respectively, as discussed elsewhere.[3,5] The spectral similarities of the three oxidation levels indicate that these mechanisms apply in the 4- and 5- clusters as well. In particular, the alternation in signs of ring proton shifts of terminal (t) ligands

Table VII. Magnetic Moments and Isotropic Shifts of $[Mo_2Fe_6S_8(SPh)_9]^z$ Clusters in CD_3CN Solutions at 296 K

		$(\Delta H/H_o)_{iso}$,[a] ppm					
z	μ (μ_B)	o-H_t[b,c]	m-H_t	p-H_t	o-H_b[b,c]	m-H_b	p-H_b
3-	5.65	+10.2	−6.61[d]	+10.8[d]	−1.42	+1.34	+1.87
4-[e]	6.24	~+11[f]	−7.55	+11.4	−0.45	+1.45	+1.88
			(−9.17)	(+13.6)	(−0.66)	(+1.75)	(+2.49)
5-	6.84	+10.8	−8.86	+11.6	−0.47	+1.42	+0.40

[a] $(\Delta H/H_o)_{iso} = (\Delta H/H_o)_{obsd} - (\Delta H/H_o)_{dia}$; the diamagnetic reference shift is taken as −7.20 ppm[16] (PhSH in CD_3CN). [b] t = terminal, b = bridging ligand. [c] Broad signals. [d] Similar values (but with different sign convention) observed in Me_2SO-d_6.[5] [e] 1.19 mM, generated by reaction 4 by using equimolar amounts of 3- and 5- clusters; shifts at 238 K in parentheses; o-H_t signal not resolved. [f] Approximate value for very broad signal.

(Table VII) is retained in the latter clusters. Shifts of m-H_t and p-H_t increase with increasing χ^M, consistent with a contact mechanism,[48] but do not scale linearly. This behavior indicates that hyperfine coupling constants in the three species do not stand in unit ratio and/or the existence of some dipolar contributions to the shifts. Signals of the 4- cluster remain singlets as the temperature is lowered to 238 K, as shown for the m-H_t resonance in Figure 11. Subcluster equivalence can be attained by intramolecular electron transfer and the intermolecular processes of reaction 3 and two-electron exchange reactions of two 4- clusters. Because of this possible complexity we have not yet undertaken a kinetic study of electron transfer in 4- cluster systems. If the m-H_t shifts of 3- and 5- species are taken as limiting values, the 4- subcluster lifetime may be estimated as $\tau \lesssim 2 \times 10^{-4}$ s. For an intramolecular process this value requires an electron-transfer rate constant $k \gtrsim 5 \times 10^3\ s^{-1}$.[49] This lower limit is $\sim 10^3$ less

(47) Papaefthymiou, G. C.; Laskowski, E. J.; Frota-Pessoa, S.; Frankel, R. B.; Holm, R. H. *Inorg. Chem.*, in press.

(48) Reynolds, J. G.; Laskowski, E. J.; Holm, R. H. *J. Am. Chem. Soc.* **1978**, *100*, 5315.

(49) Bimolecular reactions are also fast, as seen by the observation of exchange-averaged signals in systems initially containing unequal concentrations of 3- and 5- clusters (~1–2 mM). For electron exchange between two 4- species, $k \sim 10^6\ M^{-1}\ s^{-1}$ may be estimated. The one-electron self-exchange reactions $[Fe_4S_4(SR)_4]^{2-,3-}$ have $k \sim 10^6$–$10^7\ M^{-1}\ s^{-1}$: Reynolds, J. G.; Coyle, C. L.; Holm, R. H. *J. Am. Chem. Soc.* **1980**, *102*, 4350.

than the upper limit from Mössbauer spectral results at 80 K.

Summary and Conclusions

The following statements concerning the redox, structural, and electronic properties of Mo–Fe–S clusters augment those presented previously,[3] which were based on investigations[2,3] of the cluster trianion **1** only.

(i) The four-membered electron transfer series $[Mo_2Fe_6S_8(SR)_9]^z$ (z = 5– to 2–) and the five-membered series $[Mo_2Fe_6S_8(\mu_2\text{-}OMe)_3(S\text{-}t\text{-}Bu)_6]^z$ (z = 5– to 1–) have been established, in which each series member is generated by one-electron reaction of the parent double-cubane subcluster. Existence of well-defined oxidations in the last case, series 4 based on cluster **2**, is assisted by the negative shift of redox potentials effected by *tert*-butyl substituents.

(ii) Redox potentials of the couples $[Mo_2Fe_6S_8(SR)_9]^{3-,4-}$ and $[Fe_4S_4(SR)_4]^{2-,3-}$ exhibit a mutually linear dependence on substituent R (and nearly equal values at parity of R), suggesting that in the former couple the subcluster orbitals subject to population change are appreciably Fe–S in character.

(iii) The structure of the reduced cluster $[Mo_2Fe_6S_8(SPh)_9]^{5-}$ retains the double-cubane arrangement of the more oxidized species $[Mo_2Fe_6S_8(SR)_9]^{3-}$ but displays certain differences in the bridge and subcluster units. The Mo···Mo and Mo–SR distances are longer, subcluster core volumes are ~3% larger, and terminal Fe–SPh distances are increased by ~0.07 Å. The two latter differences clearly reveal subcluster reduction, and the increased terminal bond length is consistent with the qualitative orbital description in (ii).

(iv) The intense visible absorption bands of the 3–, 4–, and 5– members of electron-transfer series 1 and 4 arise from terminal-RS → $MoFe_3S_4$ core charge-transfer transitions, on the basis of monotonic high energy band shifts upon reduction. Spectra of $[Mo_2Fe_6S_8(SR)_9]^{4-}$ (R = Et, Ph) and $[Mo_2Fe_6S_8(\mu_2\text{-}OMe)_3(S\text{-}t\text{-}Bu)_6]^{4-}$ indicate the presence of inequivalent but not strictly independent subcluster chromophores.

(v) Oxidation state descriptions of Fe atoms in the subclusters of members of series 6 have been obtained from interpolation of isomer shifts at 4.2 K to the linear relationship of (mean) oxidation state/isomer shift observed for tetrahedral FeS_4 units. Isomer shift changes between 3– and 5– clusters (0.10–0.15 mm/s) are in reasonable agreement with that (0.15 mm/s) calculated from eq 7 for the proposed oxidation states in series 6. Mo oxidation states are obtained by difference using subcluster core charges. In both series it is proposed that the Mo oxidation state(s) are effectively constant. In all cases oxidation state designations are not intended as literal descriptors but only as the best available estimates of charge distribution in electronically complex clusters.[50]

(vi) The $[Mo_2Fe_6S_8(SPh)_9]^{4-}$ member of series 6 exists as a mixed subcluster species on the Mössbauer spectral time scale at temperatures up to at least 80 K. Subclusters are proposed to have the Fe mean oxidation states of the 3– and 5– series members and to be only weakly interacting, a description sensibly consistent with absorption spectral and magnetic properties at ambient temperature.

(vii) From the summarized properties, it is concluded that electronic structural changes attendant to the redox reactions of series 6 are largely confined to subcluster Fe_3 portions and associated sulfur atoms.

$[M_2Fe_6S_9(SR)_8]^{3-}$ Clusters. Four compounds whose total analyses are in very good agreement with the composition $(R'_4N)_3[M_2Fe_6S_9(SR)_8]$ (M = Mo, W) have been reported.[2,3,4,9] A single-crystal X-ray study of $(Et_3NCH_2Ph)_3[Mo_2Fe_6S_9(SEt)_8]$[2,9] has unambiguously established a double-cubane arrangement involving $MoFe_3S_4(SEt)_3$ subclusters. The Mo···Mo separation of 3.306 (3) Å is much shorter than that in $[Mo_2Fe_6S_8(SR)_9]^{3-}$ (Table V), providing a clear distinction between the two cluster types. Owing to disorder, the bridge unit could not be unequivocally defined, but there is no doubt as to the presence of three bridging atoms. From chemical analysis, simulation of EXAFS spectra, and modeling of electron density in the disordered bridge region, the cluster structure was concluded to be **3** (R = Et).

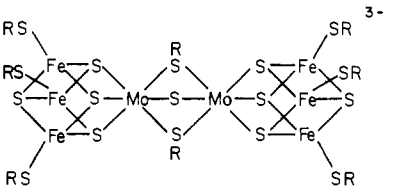

3

Certain properties of $[Mo_2Fe_6S_9(SEt)_8]^{3-,5-}$ have been examined as a comparison with those of members of series 1. (a) A four-membered electron transfer series exists whose steps are chemically reversible by CV at 100 mV/s; the potentials (Table IV) are close to those of the series based on $[Mo_2Fe_6S_8(SEt)_9]^{3-}$. (b) The absorption spectrum of the 4– cluster (λ_{max} 378 nm) differs substantially (by +(12–19)% in intensity at 378–400 nm) from the average spectrum of the 3– (λ_{max} 398 nm) and 5– (sh 348 nm) species. (c) Mössbauer parameters of the 3– and 5– clusters at 4.2 K in DMA solutions (Table VI) are essentially indistinguishable from those of $[Mo_2Fe_6S_8(SR)_9]^{3-,5-}$ under the same conditions. (The 4– cluster was not investigated.) Property c leads to the descriptions (eq 8) of the charge distributions in

$$[\alpha + \gamma]^{3-} \qquad [\beta + \epsilon]^{5-} \tag{8}$$

$$\gamma = [Mo^{4+}Fe_3^{2.67+}S_4^{2-}]^{3+}; \ \epsilon = [Mo^{4+}Fe_3^{2.33+}S_4^{2-}]$$

$[Mo_2Fe_6S_9(SEt)_8]^{3-,5-}$. These descriptions afford inequivalent subclusters, which have not been detected in Mössbauer or ^1H NMR spectra.[3] A possibility, not directly examinable by the experiments described here, is that these clusters possess an electronically delocalized Mo–S–Mo bridge unit. In this event the mean oxidation state description $Mo^{3.5+}$ is more appropriate than ones with integer oxidation states. A second possibility, raised by properties a and c, is that the bridge structure in **3** is not correct, such that the subclusters are equivalent and that the 2α and 2β descriptions in series 6 apply to the 3– and 5– clusters, respectively. This could be accomplished by, e.g., the existence of methoxide instead of sulfide in the bridge. While the available evidence does not support this proposition, a more complete demonstration of the bridge structure is desirable. This requires crystals lacking disorder in the anion; no such crystals have as yet been obtained.

The results of this and a prior[3] investigation form the basis of our current interpretation of the electronic properties Mo–Fe–S cubane-type clusters. This interpretation provides a rather elementary view of complicated molecules, further understanding of which would be assisted by the development of a theoretical electronic structural model consistent with the properties described here and elsewhere.[3] With the electronic properties of reduced clusters at a reasonable stage of definition, attention has been directed toward the synthesis of single cubane-type clusters and the reactions of reduced single and double cubanes with nit-

(50) In response to the criticism by ML,[6] this statement clarifies our position on the meaningfulness of Fe oxidation states obtained from the δ/s correlation in Figure 9. We are mindful of the small isomer shift differences among the members of series 6 and possible small perturbations of δ values from those of Fe–S species used in the correlation by the presence of Mo. The oxidation state assignments in series 6 are considered to provide a coherent view of charge distribution in oxidized *and* reduced clusters. We regard the +2.67 Fe mean oxidation state description of $[Mo_2Fe_6S_8(SR)_9]^{3-}$ to be preferable to the +2.5 ± 0.1 value of ML[6] on the basis of results presented here and elsewhere.[3] The latter value requires inequivalent subclusters in $[Mo_2Fe_6S_8(SR)_9]^{3-}$ and $[Mo_2Fe_6S_8(OMe)_3(SR)_6]^{3-}$, a situation for which there is no clear structural or spectroscopic evidence. The presence of localized subclusters in $[Mo_2Fe_6S_8(SPh)_9]^{4-}$ argues against equilibration of inequivalent subcluster electron distributions by internal electron transfer at rates fast on the Mössbauer spectral time scale. Recently, the value of +2.67 has been adopted by certain of these investigators in analyzing the magnetic properties of $[Mo_2Fe_6S_8(\mu_2\text{-}OMe)_3(SPh)_6]^{3-}$.[38] Throughout the text values of s calculated from eq 7 are quoted to three figures in order to reveal ranges of possible values afforded by small differences in isomer shifts; such values are of course significant to two figures only. The oxidation states in series 6 are arrived at from the correlation whose results are extended to the nearest mean value consistent with xFe(III) and $(3-x)$Fe(II), x = 0–3. The s values used in the fit of eq 7 are accurately defined by the compositions of the various Fe–S compounds.

rogenase substrates. The results of these investigations will be reported subsequently.

Acknowledgment. This research was supported by NSF Grants 80-06601 and 81-06017 at Harvard University and by the National Science Foundation at the Francis Bitter National Magnet Laboratory. We thank Drs. E. J. Laskowski and T. E. Wolff for experimental assistance, J. M. Berg for performing volume calculations, K. S. Hagen for useful discussions, and G. Shoham for contributing to the crystal structure determination. X-ray and NMR equipment used in this research were obtained by NSF Grants CHE 80-00670 and CHE 80-08891.

Supplementary Material Available: Crystal structure data for $(Et_4N)_5[Mo_2Fe_6S_8(SPh)_9]$: unit-weighted least-squares planes for the anion (Table S-I), positional and thermal parameters for benzenethiolate carbon atoms (Table S-II) and cation carbon and nitrogen atoms (Table S-III), and values of $10|F_o|$ and $10|F_c|$ (Table S-IV) (47 pages). Ordering information is given on any current masthead page.

Reaction of Trimethyl- and Triphenylstannate, $(CH_3)_3Sn^-$ and Ph_3Sn^-, with Optically Active 2-Octyl Bromide, Chloride, and Tosylate[1]

Joseph San Filippo, Jr.,* and Joseph Silbermann

Contribution from the Department of Chemistry, Rutgers University, New Brunswick, New Jersey 08903. *Received July 29, 1981*

Abstract: The reaction of lithium, sodium, and potassium trimethylstannate, $(CH_3)_3SnLi$, -Na, and -K, and triphenylstannate, Ph_3SnLi, -Na, and -K, with optically active 2-octyl tosylate, chloride, and bromide is reported. Alkylation of $(CH_3)_3SnM$ with 2-octyl tosylate proceeds with complete inversion at carbon. The corresponding reactions with 2-octyl chloride and especially 2-octyl bromide show considerably greater variations in reaction stereoselectivity. These variations depend on a variety of reaction parameters, including the order of reagent addition, i.e., normal vs. inverse addition of reagents, reaction temperature, solvent, gegenion, concentration, and additives. Thus, for example, at 0 °C the normal addition reaction of 2-octyl chloride with $(CH_3)_3SnM$ in THF proceeds with 100% inversion of configuration, while the equivalent reactions with 2-octyl bromide proceed with 34% (M = Na), 33% (M = K), and 53% (M = Li) *net* inversion. The latter reactions are more stereoselective when carried out at lower temperatures: at −70 °C the corresponding values are 62% (M = Na) and 83% (M = Li) *net* inversion. Stereoselectivity in these reactions is dramatically influenced by the order of reagent addition. Thus, under inverse-addition conditions, for example, the reaction of $(CH_3)_3SnM$ with 2-octyl bromide in THF at 0 °C occurs with high stereoselectivity (97% and 98% net inversion, respectively, for M = Li and Na) and with minor adjustment of other parameters can be made to occur stereospecifically. Both the normal and the indirect addition of Ph_3SnLi and -Na to 2-octyl bromide occur with complete inversion of configuration at carbon. A comparison of the reactivity of $(CH_3)_3SnM$ and Ph_3SnM reveals that the latter is significantly less reactive than the former; triphenylstannate, however, is the more stereoselective reagent, its reaction with optically active 2-bromooctane being essentially stereospecific, irrespective of the order of reagent addition. The results of this study and those from earlier investigations involving the *cis*- and *trans*-4-*tert*-butylcyclohexyl and cyclopropylcarbinyl systems are compared and discussed as well as the reliability of recently reported trapping experiments for discerning between the S_N2 and free radical components of such reactions.

In earlier reports we presented the results of our investigations of the reaction of selected metalate anions with various alkyl halides.[2] These studies revealed, inter alia, that the course of these reactions varies substantially with the nature of the leaving group. Thus, for example, *cis*- and *trans*-4-*tert*-butylcyclohexyl tosylates react with Me_3SnLi in THF at 0 °C to afford, respectively, *trans*- and *cis*-(4-*tert*-butylcyclohexyl)trimethyltin corresponding to complete inversion of configuration at carbon. By comparison, the corresponding reaction with *cis*- and *trans*-4-*tert*-butylcyclohexyl bromide produces a mixture of these products exhibiting essentially complete loss of stereochemical integrity.

As a stereochemical probe, the 4-*tert*-butylcyclohexyl system suffers from certain limitations which do not attend the use of an optically active substrate. We report here the results of our investigation of the reaction of optically active 2-octyl tosylate, chloride, and bromide with $(CH_3)_3SnM$ and Ph_3SnM, along with several related findings.

Results

Preparation of Optically Pure 2-Octyltrimethyltin and 2-Octyltriphenyltin. In order to employ traditional experimental procedures (i.e., polarimetry), it was necessary to establish the absolute rotation of optically active 2-octyltrimethyltin, **1**. The fact that the optical resolution of such a substance is impractical requires that a stereospecific synthesis of **1** be available. On the basis of our previous observation that the reaction of $(CH_3)_3SnLi$ with both *cis*- and *trans*-4-*tert*-butylcyclohexyl tosylate proceeds with essentially complete (>99%) inversion of configuration,[2] it seemed reasonable to expect that the corresponding reaction with the tosylate of optically active 2-octanol would occur with equivalent stereochemical integrity. As seen below, the reaction of lithium trimethylstannate with the tosylate of (−)-(*R*)-2-octanol does yield optically active **1**. Of course, this result does not establish that the observed rotation is the maximum value. We attempted to establish this fact by carrying out the equivalent synthesis by an independent route.

$$(-)\text{-}(R)\text{-}2\text{-}C_8H_{17}OH \xrightarrow[py]{TsCl} (-)\text{-}(R)\text{-}2\text{-}C_8H_{17}OTs \quad (1)$$

$$(-)\text{-}(R)\text{-}2\text{-}C_8H_{17}OTs + (CH_3)_3SnLi \xrightarrow[-78\ °C]{THF} (+)\text{-}(S)\text{-}2\text{-}C_8H_{17}Sn(CH_3)_3 \quad (2)$$

(*S*)-1, $[\alpha]^{25}_D$ + 26.1° (neat)

Lithium diorganocuprates have been extensively employed as reagents for the production of carbon–carbon σ bonds by reaction

(1) Supported by the National Science Foundation, Grant 80-17405, and DOE, Contract DE-AS05-80ER-1062.

(2) San Filippo, J., Jr.; Silbermann, J.; Fagan, P. J. *J. Am. Chem. Soc.* **1978**, *100*, 4834.

0002-7863/82/1504-2831$01.25/0